Challenges and Strategies for Optimization of Glycerol Steam Reforming Process

Joel M. Silva[1], M. A. Soria[1,], Luis M. Madeira[1,*]*

[1] LEPABE, Department of Chemical Engineering, Faculty of Engineering, University of Porto, Rua Dr. Roberto Frias s/n, 4200-465 Porto, Portugal

* Corresponding Authors. masoria@fe.up.pt (MA Soria) and +351-225081519 / mmadeira@fe.up.pt (LM Madeira)

Abstract

The steam reforming of the main biodiesel by-product, glycerol, has been catching up the interest of the scientific community in the last years. The use of glycerol for hydrogen production is an advantageous option not only because glycerol is renewable but also because it's use would lead to the decrease of the price of biodiesel, thus making it more competitive. Consequently, the use of biodiesel at large scale would significantly reduce CO_2 emissions comparatively to fossil fuels. Moreover, hydrogen itself is seen as a very attractive clean fuel for transportation purposes. Therefore, the industrialization of the glycerol steam reforming (GSR) process would have a tremendous global environmental impact. In the last years, intensive research regarding GSR thermodynamics, catalysts, reaction mechanisms and kinetics, and innovative reactor configurations (sorption enhanced reactors (SERs) and membrane reactors (MRs)) has been done, aiming for improving the process effectiveness. In this review, the main challenges and strategies adopted for optimization of GSR process are addressed, namely the GSR thermodynamic aspects, the last developments on catalysis and kinetics, as well as the last advances on GSR performed in SERs and MRs.

Keywords: glycerol; steam reforming; catalyst; kinetics; sorption enhanced reactor; membrane reactor.

Table of Contents

Notation and Glossary

E_a	Activation energy
$E_{a,Pd}$	Activation energy of a Pd-based membrane
f	Fraction of H_2 removal
G	Gibbs free energy
J_{H_2}	Flux of H_2 through the membrane
K	Equilibrium constant
k	Reaction rate constant
K_i	Adsorption constant of component i
k_0	Pre-exponential factor
k_C	Coke deposition reaction rate constant
n_i	Molar number of component i
$p_{H_2,permeate}$	Partial pressure of H_2 in the permeate side
$p_{H_2,retentate}$	Partial pressure of H_2 in the retentate side
p_i	Partial pressure of component i
P_{Pd,H_2}	Permeability of a Pd-based membrane to H_2
P^0_{Pd,H_2}	Pre-exponential factor
R	Ideal gas constant
$r_{coke\ deposition}$	Reaction rate of coke deposition
r_{GSR}	Reaction rate of glycerol steam reforming
T	Absolute temperature
X_1, X_2	Basic and acid active sites, respectively

Greek letters

δ	Membrane thickness
ΔH^0	Standard enthalpy
$\Delta H_r^{298\ K}$	Reaction enthalpy at 298 K
μ_i	Chemical potential of component i

Superscripts

a, b	Partial reaction orders for glycerol and steam, respectively
x	Pressure exponent

List of acronyms

CTAB	Cetyltrimethyl Ammonium Bromide
CVD	Chemical Vapor Deposition
EP	Electroless Plating
GHSV	Gas Hourly Space Velocity
GSR	Glycerol Steam Reforming
IUPAC	International Union of Pure and Applied Chemistry
MR	Membrane Reactor
PEMFC	Polymer Electrolyte Membrane Fuel Cell
PSA	Pressure Swing Adsorption
PSS	Porous Stainless Steel
SEGSR	Sorption-Enhanced Glycerol Steam Reforming
SER	Sorption-Enhanced Reactor
SRM	Steam Reforming of Methane
TR	Traditional Reactor
WGFR	Water/Glycerol Feed Ratio (molar)

WGS	Water-Gas Shift
WHSV	Weight Hourly Space Velocity
YSZ	Yttria-Stabilized Zirconia

1 Introduction

Biodiesel is a promising alternative energy source because it is a renewable fuel and reduces greatly CO_2 emissions compared to fossil fuels (Fig.1). The production of biodiesel is most commonly done through transesterification with methanol of triglycerides extracted from sunflower oils, soybean and rapeseed (Fig. 2). This process produces glycerol as the main by-product (100 kg of glycerol/tone of biodiesel) [1, 2]. Moreover, the annual worldwide production of biodiesel has been in an increasing trend lately, as can be seen in Fig. 3 [3]. However, biodiesel is not competitive in terms of price yet [4]. One way of lowering the production cost of biodiesel would be to use its main by-product, glycerol, to produce H_2 (or syngas) via steam reforming, for example, thus providing an extra value to such a waste.

Hydrogen is a clean energy source with numerous uses and its demand is expected to greatly increase in the future, mainly due to the technological advancements in the fuel cell industry. Nowadays, nearly 48% of the worldwide produced hydrogen is generated through the steam reforming of methane (SRM), while the reforming of naphtha/oil contributes with 30%, the coal gasification with 18% and electrolysis with only 3.9% [5]. The SRM, in particular, consists of CH_4 reacting with H_2O to yield syngas at high temperatures (700-1100 °C) [4]. Stoichiometrically, 3 moles of H_2 can be obtained per mole of methane through SRM, while 7 moles of H_2 can be extracted from 1 mol of glycerol through glycerol steam reforming (GSR), as presented in eq. (1).

$$C_3H_8O_3 + 3H_2O \leftrightarrow 7H_2 + 3CO_2 \qquad (\Delta H_r^{298\,K} = 128 \text{ kJ·mol}^{-1}) \qquad (1)$$
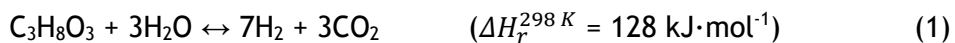
Furthermore, while for SRM a fuel (CH_4) is consumed to produce another fuel, the same thing does not happen for GSR. Therefore, the use of glycerol instead of methane would be advantageous [4]. Even though steam reforming is the main target of focus in this review, there are other methods to convert glycerol into H_2:

- Auto-thermal reforming [6-8];
- Partial oxidation gasification [9-11];
- Aqueous-phase reforming [12-14];
- Supercritical water reforming [15-17].

The reason why GSR was chosen as focus of study instead of any of the other processes is mainly due to the fact that the steam reforming process is widely used in industry and it would not require many changes in the system if the feedstock was changed from natural gas or naphtha to glycerol [4].

The GSR process, like any other process, has some challenges that need to be overcome in order to accomplish its effective commercialization. Some of the main challenges are:

- The GSR is an endothermic reaction, thus requiring high temperatures and inherently high operating costs. Furthermore, more resistant reactors would be needed and so higher capital costs would be involved;

- The GSR process has side reactions, which affect both production and purity of H_2. The main side reactions represented by eq. (2, 3 and 4) lead to methane formation either by reaction of carbon monoxide and hydrogen or reaction of carbon dioxide and hydrogen or through hydrogenolysis of glycerol, respectively.
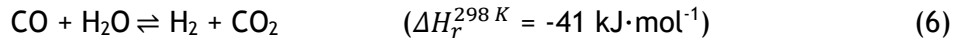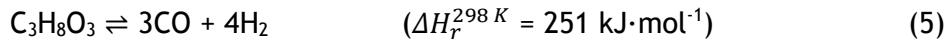
$$CO + 3H_2 \leftrightarrow CH_4 + H_2O \qquad (\Delta H_r^{298\,K} = -206\ kJ \cdot mol^{-1}) \qquad (2)$$

$$CO_2 + 4H_2 \leftrightarrow CH_4 + 2H_2O \qquad (\Delta H_r^{298\,K} = -165\ kJ \cdot mol^{-1}) \qquad (3)$$

$$C_3H_8O_3 + 2H_2 \leftrightarrow 2CH_4 + CO + 2H_2O \qquad (\Delta H_r^{298\,K} = -160\ kJ \cdot mol^{-1}) \qquad (4)$$
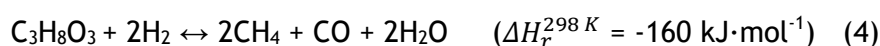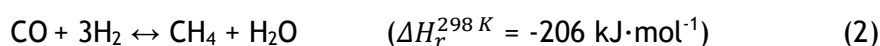
- Although 7 moles of hydrogen should theoretically be produced per each mole of glycerol that reacts, many authors have observed upper H_2 yield limits lower than 7 [18-23];

- The GSR is a thermodynamically-limited reaction (eq. (1)), being inherently the conversion detrimentally affected in certain conditions, particularly at lower temperatures [24];

- The formation of coke is also an issue since it deactivates the catalyst, thus affecting H_2 yield and purity and long term operation;

- Besides producing hydrogen the GSR reaction also produces carbon dioxide, whose release is target of environmental concern and restricted by legislation.

With the aim of addressing these problems, new catalysts have been developed and different purification methods have been studied. Moreover, new reactor configurations combining the GSR reaction and hydrogen or carbon dioxide selective removal have also been target of intense research, due to their potential to solve some of the limitations previously mentioned. In this review some of the important developments regarding the GSR reaction (including thermodynamics, developed catalysts and reaction kinetics) and its combination with a hydrogen perm-selective membrane or a CO_2 sorbent, in the perspective of process intensification, are reviewed. Up to the authors' knowledge, a review that conjugates a literature survey of all these subjects is still missing.

2 Thermodynamics of GSR – Influence of different parameters

2.1 Conventional GSR

The GSR is an equilibrium-limited process, as previously mentioned, that involves the decomposition of glycerol followed by the water-gas shift (WGS) reaction:

$$C_3H_8O_3 \rightleftharpoons 3CO + 4H_2 \qquad (\Delta H_r^{298\,K} = 251 \text{ kJ·mol}^{-1}) \qquad (5)$$

$$CO + H_2O \rightleftharpoons H_2 + CO_2 \qquad (\Delta H_r^{298\,K} = -41 \text{ kJ·mol}^{-1}) \qquad (6)$$

In order to maximize the production of hydrogen, one must first fully understand how the thermodynamic boundaries are influenced by the different parameters.

There are several studies focused on the thermodynamics of the GSR [24-31]. One of the most important parameters affecting any reaction system is temperature. Once glycerol decomposition is highly endothermic and requires more heat than that produced in the WGS reaction, the overall GSR process is endothermic (eq. (1)), thus meaning that higher temperatures benefit the H_2 production (glycerol conversion, H_2 yield and selectivity) (Fig. 4) [24]. Mathematically, the equilibrium of a system at constant pressure and temperature is given as follows:

$$dG = \sum_{i=1}^{K} \mu_i dn_i = 0 \qquad (7)$$

where G is the Gibbs free energy, μ_i is the chemical potential of component i and n_i is the number of moles of component i in the system. The goal is to determine the set of n_i values that minimize de value of G (thermodynamic equilibrium). There are two different thermodynamic approaches that can be used to solve this: (i) stoichiometric [30, 32, 33] and (ii) nonstoichiometric [24-28, 31, 34-38]. By using the stoichiometric approach a set of stoichiometrically independent reactions, which are normally chosen arbitrarily from a set of possible reactions, is used to describe the system. Instead, if the nonstoichiometric method is used the equilibrium composition is calculated based on the direct minimization of the Gibbs free energy of a specific set of species [27]. Both methods have their own advantages, however there has been a significant tendency towards the nonstoichiometric one. In fact, the use of the latter does not require a selection of the possible set of

reactions. Moreover, during computation there is no divergence and there is no need of an accurate initial estimation of the equilibrium composition [27].

Since the GSR is an endothermic process ($\Delta H^0 > 0$), if higher temperatures are used more hydrogen is produced, thus confirming the trend in Fig. 4. Furthermore, a variation of the number of moles of all products (H_2, CO, CO_2 and CH_4) with temperature is also observed in this figure. At lower temperatures, the formation of H_2, CO_2 and CH_4 as main products is seen. This might be due to the fact that the exothermic WGS and methane formation reactions are mainly favored at low temperatures. In contrast, endothermic reactions like GSR and reverse WGS are more favored at higher temperatures. This could explain the increase of both H_2 and CO contents and the small decrease of CO_2 observed at those temperatures. In any case, an optimum high temperature is normally determined. However, higher temperatures are not favorable from the economic point of view and so alternative ways to attain high H_2 production yields have to be considered.

The molar water/glycerol feed ratio (WGFR) has also been found to highly influence the production of H_2 (mainly the H_2 yield and selectivity) in the equilibrium. Considering the Le Chatelier's principle, it is expectable that for higher WGFRs the equilibrium shifts towards the consumption of the excess of water, thus producing more hydrogen. Such a behavior has been indeed verified and, as can be seen in Fig. 5, the H_2 yield increases as the WGFR increases from 4 to 15, whatever the temperature. For WGFRs above 9 the H_2 yield increases at a slower rate, especially at higher temperatures. However, the amount of water used should not be too high due to the excessive vaporization costs that it would bring at industrial scale. Moreover, it should be chosen taking into consideration the H_2O activation capacity of the catalyst used and the other operating conditions (temperature and pressure).

The influence of both operation temperature and WGFR on the formation of coke has been investigated as well [25, 28, 39]. Adhikari *et al*. [28] suggest that carbon formation may happen through the following reactions:

$$2CO(g) \leftrightarrow CO_2(g) + C(s) \qquad\qquad (8)$$

$$CH_4(g) \leftrightarrow 2H_2(g) + C(s) \qquad\qquad (9)$$

$$CO(g) + H_2(g) \leftrightarrow H_2O(g) + C(s) \qquad\qquad (10)$$

$$CO_2(g) + 2H_2(g) \leftrightarrow 2H_2O(g) + C(s) \tag{11}$$

Fig. 6 [25] shows that, in order to avoid carbon formation, which poisons the catalysts, high WGFRs and temperatures should be used. In fact, for WGFRs higher than 5, carbon formation is completely inhibited for all the temperature range considered (550-1000 K). These results are in line with those obtained by Adhikhari *et al*. [28] and Authayanun *et al*. [39].

Pressure is also an important parameter because it has a significant influence on the performance of reaction systems. That influence is even more noticeable for processes during which there is variation of the total number of moles, like the GSR, since it affects the thermodynamic equilibrium (Le Chatelier's principle). For the case of GSR, higher pressures lead to a lower hydrogen production in the equilibrium. Moreover, enhanced formation of methane has also been verified [25, 28-30]. Therefore, it results to be advantageous to use lower pressures not only because it is economically more attractive (as far as the pressure is not too low) but also because it leads, under equilibrium, to higher H_2 production (Fig. 7) [26]. Pressures lower than the atmospheric pressure would be desired, however, these pressures are more difficult to attain under economically attractive conditions in industrial practice. An alternative way to achieve this would be to use a carrier gas to dilute the reactants, thus decreasing their partial pressures. Chen *et al*. [26] came to the conclusion that by increasing the amount of carrier gas, not only the maximum H_2 production increased but also the optimum temperature dropped. Although it may seem a good solution, at industrial scale it is not so attractive since it would require complex separation processes after the reactor.

In sum, it is clear that high temperatures, high WGFRs and low pressures favor hydrogen production in the equilibrium. Temperatures between 580-702 °C, WGFRs between 9-12 and atmospheric pressure have been reported in the literature as optimum conditions [25-27, 29].

2.2 GSR with CO_2 Adsorption

It is clear that even at favorable conditions, the GSR equilibrium is still quite limiting in terms of H_2 yield, for example. For the cases analyzed in the previous section, the maximum H_2 yields observed were close to 6, due to the co-existence of several reaction apart GSR. However, according to the GSR reaction stoichiometry (eq. (1)), a maximum

H_2 yield close to 7 can be obtained. Such a yield could be reached by performing GSR simultaneously with CO_2 capture, since the selective removal of CO_2 shifts the thermodynamic equilibrium towards higher H_2 yields. The Sorption Enhanced Glycerol Steam Reforming (SEGSR) process also allows to work at milder operating conditions, thus leading to lower operation costs. Moreover, since the emissions of CO_2 are diminished, the SEGSR can be considered as a good solution as long as there is a way to store/valorize captured CO_2 [40]. In this section a review of some thermodynamic studies on SEGSR is done.

Different approaches have been used to account for CO_2 sorption in thermodynamic simulations. Wang *et al*. [41] accounted for 17 species in SEGSR among which 13 were gases and 4 were solids. These solids include carbon, CaO, $CaCO_3$ and $Ca(OH)_2$. It is assumed that, in the presence of a CO_2 sorbent like CaO, the following reactions take place:

$$CaO(s) + CO_2(g) \leftrightarrow CaCO_3(s) \qquad\qquad\qquad (12)$$

$$CaO(s) + H_2O(g) \leftrightarrow Ca(OH)_2(s) \qquad\qquad\qquad (13)$$

$$Ca(OH)_2(s) + CO_2(g) \leftrightarrow CaCO_3(s) + H_2O \qquad\qquad\qquad (14)$$
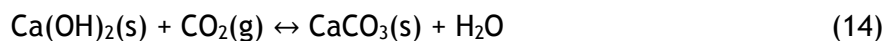
In Fig. 8 [41] the effect of temperature and WGFR on the equilibrium concentration of H_2 (dry basis) during (a) GSR and (b) SEGSR is presented. For the first case, the observed behavior is very similar to what has already been discussed in the previous section. Regarding the SEGSR, it can be observed that for increasing WGFR values, at constant temperature, the equilibrium hydrogen concentration also increases for the reason stated before. Therefore a balance should be sought, being that a value of 9 is proposed by Chen *et al*. [42] and Silva *et al*. [43] as the most favorable for hydrogen production. In terms of temperature, a more noticeable effect is observed. While for temperatures between 500-900 K and constant WGFR there is an increase of the equilibrium hydrogen concentration, for temperatures above 900 K this concentration decreases. The authors suggest that the increase of the H_2 concentration up to 900 K is associated to the compromise between eq. (2, 5, 6, 12, and 13). The decrease of the equilibrium hydrogen concentration observed thereafter is due to the fact that the CO_2 sorption described by eq. (12) is inhibited due to its exothermic nature. By comparing Fig. 8 (a) and (b), it is clear that the removal of CO_2 during reaction enhances H_2 production (Le Chatelier's principle), especially at lower

temperatures where CO_2 sorption is more intense. Chen *et al.* [42] observed that, while without CO_2 capture the maximum H_2 yield, at WGFR of 9 and 1 atm, was 6, H_2 yields of approximately 6.5 and 7 were obtained when 80% and 99% of the CO_2 was removed, respectively. Moreover, the increment of H_2 production due to CO_2 removal is higher for lower temperatures, which is related with the fact that lower temperatures favor CO_2 capture.

Regarding the variation of the concentration of CO_2, Wang *et al.* [41] observed very similar behavior between GSR and SEGSR at temperatures above 900 K. However, at temperatures below 900 K the CO_2 concentration was much lower in the SEGSR due to the already mentioned enhanced sorption, despite the higher CO_2 production (Le Chatelier's principle). On the other hand, the production of both methane and carbon monoxide is lower in the SEGSR.

Chen *et al.* [44] varied the operation pressure between 1-20 atm and analyzed its effect on both GSR and SEGSR in terms of hydrogen yield. The first thing that the authors noticed was that the H_2 yield decreased with increasing pressures for both processes. However, the SEGSR was less sensitive to pressure than GSR. This happens because, even though higher pressures do not favor SEGSR but methanation instead, higher pressures enhance CO_2 adsorption. For this reason, the negative effects of pressure are diminished during SEGSR, being that the increment in the production of H_2 due to CO_2 removal is more noticeable at higher pressures.

The sorbent/glycerol ratio is also an important parameter to be taken into consideration. The concentration of H_2 increases for increasing CaO/glycerol ratios, while the concentrations of both CO and CO_2 highly decrease [41]. The concentration of methane presents a maximum. However, for increasing CaO/glycerol molar ratios above 10, there is almost no variation of H_2, CO, CO_2 and CH_4 concentrations. Therefore, 10 may be considered the optimum CaO/glycerol molar ratio.

Finally, the deposition of carbon has also been target of investigation. As already discussed for GSR, high temperatures and WGFRs inhibit coke formation. Wang and co-authors observed higher carbon deposition in GSR than in SEGSR. Therefore it can be concluded that the capture of CO_2 inhibits coke formation. This is supported by the lower concentrations of CO and CO_2, which origin coke formation, during SEGSR (eq. (8, 10, and 11)). On the other hand, by analyzing Fig. 9 [41] it can be observed, for SEGSR, that at 1 atm coke is completely absent at temperatures above 500 K and WGFRs higher than 1.8.

By increasing the pressure from 1 to 50 bar, the formation of a second carbon formed region occurs. This might be because of the enhancement of the reactions in eq. (8, 10, and 11). In this case coke formation is only completely avoided at WGFRs above 3 (again for temperatures above 500 K). In another work, Silva *et al*. [43] concluded that even using a WGFR as low as 1.5, it would be possible to work at temperatures below 885 K (1 atm) without any carbon formation. Furthermore, in order to eliminate the possibility of carbon formation in all the temperature range (500-1400 K) under atmospheric pressure, WGFRs higher than 2 would have to be used. This value is very similar to the one reported by Wang *et al*. [41] – Fig. 9.

2.3 GSR with H_2 Removal

The removal of hydrogen from the reaction medium instead of CO_2 is another possibility that has been target of some interest. Analogously to the SEGSR, the selective removal of H_2 during GSR by means of a membrane reactor (MR) also shifts the thermodynamic equilibrium towards higher H_2 yields. Moreover a highly pure H_2 stream, which is suitable to be used in polymer electrolyte membrane fuel cells (PEMFCs), is generated. There have been several studies that have focused on the experimental assessment of GSR in MRs, however the study of the thermodynamic behavior of the process has seldom been done. A revision of such work is briefly reported in this section.

Wang *et al*. [45] investigated the effect of temperature, WGFR, pressure and fraction of hydrogen removal on a MR. Regarding the operation pressure, it was found that higher pressures benefit the permeation of hydrogen through the membrane due to the increase of the driving force. However, the thermodynamics of GSR is not favored by high pressures as already discussed. The authors observed that superior hydrogen production occurs at 1 atm and, for that reason, all the analysis was performed at this pressure. Fig. 10 [45] depicts the influence of both temperature and WGFR on the production of H_2 through GSR in a MR. It is observable that, as expected, the increase of both temperature and WGFR provoke an enhancement in the production of hydrogen. However, H_2 production reaches a maximum at a certain temperature and then starts decreasing for higher temperatures (such effect is not verified for H_2 removals of 99% and 100%). Regarding the fraction of H_2 removal, removing more hydrogen shifts the thermodynamic equilibrium towards higher hydrogen production according to the Le Chatelier's principle. Moreover, higher H_2 removal dislocates the maximum hydrogen production to lower

temperatures (Fig. 10a). While with no H_2 removal the maximum H_2 yield is approximately 6 at 925 K, the maximum yield becomes close to 7 at 825 K for 80% of H_2 removal, and with fractional hydrogen removal of 0.99 and 1, the H_2 yield is close to 7 for all range of temperatures considered. The same is verified for all range of WGFRs considered (Fig.10b). Furthermore, the increase in H_2 production when the WGFR increases from 9 to 12 is very small. Consequently, the optimum conditions for GSR in the MR were found to be 825-875 K, WGFR of 9 and 1 atm. The formation of both CO and CH_4 is decreased by selectively removing H_2.

The formation of carbon was also analyzed by Wang *et al*. [45]. As can be seen in Fig. 11 [45], a WGFR value of 4.5 is enough to completely inhibit carbon formation for all range of temperatures and fractions of hydrogen removal tested. With exception to the case of fractional H_2 removal of 0.99, the minimum WGFR required to avoid carbon formation decreases slightly with the increase of temperature up to 800 K. From that point on, the decrease with temperature is much faster and from approximately 873 K on, the influence of the H_2 removal fraction on the minimum WGFR is practically negligible. For a fraction of hydrogen removal of 0.99 the minimum WGFR required to inhibit carbon formation decreases very rapidly. By comparing the different levels of hydrogen removal, it can be observed that higher hydrogen removal leads to higher minimum WGFRs necessary to inhibit carbon formation, except for 99% hydrogen removal (where the minimum WGFR necessary to avoid carbon formation becomes lower than that for lower hydrogen removal fractions at temperatures lower than 923 K). In any case, if the optimum WGFR of 9 is used, no problems with carbon formation will exist.

3 GSR catalysts developments

In the last decade extensive research has been done regarding the heterogeneous catalysis of the GSR reaction for either synthesis gas or H_2 production. The most investigated materials until now have been Ni, Pt, Co and Ru-based catalysts. Other less researched materials like Rh, Ir and Pd have also shown interesting attributes. Among the above mentioned catalysts, Ni-based catalysts, as non-noble metal-based catalysts, have been extensively studied. At the moment, the main goal is to design highly reducible and with high oxygen mobility redox catalysts for low-temperature GSR [46].

3.1 Ni-based Catalysts

Nickel catalysts for the GSR have been extensively studied over the last years. A big advantage that Ni catalysts present when compared to the noble metal-based ones is their lower price.

3.1.1 Effect of the support on the catalytic performance

It has been found that the use of different supports in Ni-based catalysts results in much different catalytic performances [47-51]. Table 1 summarizes the catalytic performance and operating conditions of different Ni-based catalysts on GSR. Adhikari *et al*. [48] compared the performance of Ni catalysts on different supports: MgO, CeO_2 and TiO_2. At 600 °C and WGFR of 9, it was observed the following order of H_2 selectivity: CeO_2 (70%) > MgO (40%) > TiO_2 (15%). Moreover, the ceria supported catalyst was found to present the lowest carbon deposition. It was suggested that ceria establishes a better interaction with the nickel active phase, which leads to a higher metal dispersion and inherently available surface area. Pant *et al*. [50] observed that the presence of ceria affects the reduction of Ni^{2+} species, thus enhancing the catalyst activity. It has also been suggested that the dual oxidation state (+4/+3) that ceria presents leads to oxygen release which reacts with the carbon that is deposited, thus reducing coke formation [15, 52-55]. Moreover, Ni/CeO_2 catalyst is able to enhance both methane reforming and WGS reaction and presents high hydrogen selectivity through GSR [28, 56-58]. Also, it has been reported that the H_2 yield is highly dependent on the nature of the active phase as well as its interaction with ceria [28, 56, 57, 59].

The acidic character of TiO_2 is responsible for the higher coke formation on Ni/TiO_2, which leads to a worse GSR performance [48]. Nichele *et al.* [51] showed that Ni/TiO_2 has very low activity in C-C bond rupture, even at high temperatures, and that the contribution of the WGS reaction is even smaller. This is due to the fact that anatase, where nickel ions are incorporated after being oxidized and then reduced under H_2 flow, is stable only at relatively low temperatures and its weak interaction with Ni is not able to avoid re-oxidation of the metallic active phase in the steam reforming conditions [51].

Sánchez *et al.* [49], Pant *et al.* [50] and Adhikari *et al.* [56] analyzed the performance of Ni/Al_2O_3 catalysts for the GSR. The first group observed catalyst deactivation after 8h time on stream (at 600 and 650 °C). Wen *et al.* [61] verified that Ni-Al_2O_3 supported catalysts undergo quick deactivation. However, as already stated, deactivation is highly dependent on, among another things, the support nature. Many authors have verified the formation of carbonaceous deposits over Ni/Al_2O_3, which led to relatively fast catalyst deactivation [49, 50, 61, 62]. Normally, the formation of coke deposits is associated to dehydration, cracking and polymerization reactions which take place on the acid sites of alumina [63]. Besides presenting higher carbon deposition, Pant *et al.* [50] also concluded that the prepared Ni/Al_2O_3 catalyst presented higher catalyst sintering than the Ni-ceria supported one. It has been suggested that the sintering of the Ni active phase is associated to a transition of alumina to crystalline phase during reaction [64].

Nichele *et al.* [51] also tested a Ni/ZrO_2 catalyst, having concluded that it presented high surface area, high stability at 650 °C and strong interaction of the support with the metal phase. Also, it was found that for lower temperatures (500 °C) the zirconia supported catalyst was even more active. However, there was a lower stability. In the same work a Ni/SBA-15 was also used, having presented insufficient hydrothermal resistance, which led to catalyst deactivation. However, sintering was avoided since it provided a good stabilization of the Ni active phase.

Nickel supported on neutral SiC has been reported to present outstanding stability and high yield of syngas [60]. The neutral nature of this material promotes an intrinsic nickel contribution to GSR, especially in terms of dehydrogenation and decarbonylation. Simultaneously, SiC leads to minimal side reactions from the condensation and the dehydration induced by the basic and acid properties, respectively. Because of this, the Ni/SiC catalyst is able to present high stability for GSR and low carbon deposition.

It is, therefore, evident that the nature of the support affects mainly the stability of the active phase. In order to reach a highly stable active phase, strong interactions between the metal phase and the support are required. These strong interactions also lead to higher activity and selectivity.

3.1.2 Effect of the addition of a promoter on the catalytic performance

In many studies reported in the literature, promoters have been used in Ni-supported catalysts in order to improve their performance towards the GSR reaction. Table 2 presents, in summary, the effect of the promoter on the catalytic activity.

As previously mentioned, ceria presents good characteristics for GSR, having for that reason been used by many authors as a promoter [53, 67-69]. In general the addition of CeO_2 promoter enhances the activity of the non-promoted catalyst. This is mainly related to the capacity of ceria to stabilize the nickel active phase and to promote the steam reforming of the oxygenated hydrocarbons intermediates, thus leading to a reduction of coke deposition. It has also been suggested that Ce inhibits secondary dehydration reactions, which are normally favored by the presence of support acid sites, which lead to the formation of hydrocarbons that are coke precursors and generate fast catalyst deactivation [68]. It is, nonetheless, important to notice that the ceria loading must not be too high. Iriondo *et al.* [53] suggest that for a 20 wt.% ceria promoter content on alumina, ceria tends to interact with alumina instead of Ni, thus decreasing the stabilization of the nickel active phase and lowering the available surface for Ni dispersion. In the same way, it is also possible that the bigger size of ceria crystallites could also diminish the interaction between ceria and nickel active phase [70]. On the other hand, Cui *et al.* [54] showed that the activity of the $La_{0.3}Ce_{0.7}NiO_3$ mixed oxide catalyst for GSR is enhanced compared to $LaNiO_3$ catalysts and that its performance is comparable to that of a noble metal like Pt [54].

The use of ZrO_2 as a catalyst modifier has also been reported as an alternative promoter [18, 65, 67, 68], despite the fact that ZrO_2 alone is not very active for steam reforming [71]. Iriondo *et al.*[67] observed that the addition of zirconia promoter to alumina not only enhanced the performance of the non-promoted catalyst but also presented better GSR performance than the ceria-promoted catalyst. The addition of an intermediate ZrO_2 content [65, 72, 73] enhanced the H_2 yield and the capacity of the catalyst to reform intermediate products (thus suppressing secondary reactions), even at

500 °C, due to the enhancement of H_2O activation by ZrO_2. It is suggested that this improvement is associated to the formation of ZrO_2-Al_2O_3 species, which facilitates the reduction of Ni^{2+} [65]. Pant and co-workers [18] came to similar conclusions after performing GSR over a ZrO_2-promoted Ni/CeO_2 catalyst. Zirconia is able to make the ceria support more crystalline, consequently improving the metal dispersion. It is also known that, in general, ZrO_2 inhibits sintering of metallic active sites in the presence of water at high temperatures [64].

With the aim of reducing the acidity of alumina supports, thus preventing metal sintering and catalyst deactivation, alumina supports have been modified with basic La_2O_3 [22, 66, 67, 74, 75]. It has also been reported the performance of a Ni/SiO_2 modified with La_2O_3 for the GSR [76]. The combination of SiO_2, which is known to present large surface area and weak acidity, and La_2O_3, favored the formation of H_2 and CO_2 and reduced carbon formation. This decrease in the carbon formation with increasing La_2O_3 content was due to the formation of a La carbonate that removes C species deposited on the nickel sites. Therefore, the 30 wt.% (highest La_2O_3 content used) La_2O_3 catalyst presented itself as promising system for GSR, since it was stable (Fig. 12) [76], while presenting good glycerol conversion, good H_2 yield and low carbon formation.

The addition of basic Mg(II) to Ni/Al_2O_3 catalysts has been reported to prevent carbon formation by favoring both the adsorption of H_2O, O_2, CO_2 or –OH fragments and the spillover of such fragments from the support to the metal particles [20, 77, 78], thus facilitating carbon gasification. Moreover, the use Mg(II) promoter in Ni/Al_2O_3 materials enhances the stability of Ni against sintering, since it decreases the degree of interaction of Ni with alumina through intercalation between the nickel active phase and alumina. Consequently, the incorporation of nickel in the alumina phase is inhibited [67]. It has been found that the use of low amounts of Mg(II) promoter leads to higher metal dispersion, thus favoring glycerol conversion into gaseous products, while higher loadings result in lower coke deposition [20]. Other basic promoters such as Mo [66, 79-83] and Ca [66, 69, 79] have also been reported to enhance the GSR performance of non-promoted catalyst, for the same reasons previously mentioned for basic modifiers. Huang et al. [66] observed that the simultaneous presence of Mo-La-Ca inhibits the interaction between nickel and the commercial Ca-containing Linde-type 5A zeolite support, thus resulting in a remarkable stability during GSR (no deactivation during 100 h time-on-stream). Gong and co-workers [84] verified that the synergetic effect caused by the partial substitution

of La by Ca in the perovskite structure leads to enhanced metal dispersion and stronger metal-support interaction.

Hakim *et al*. [85] studied the GSR reaction over hydroxyapatite-supported Ni-Ce-Cu catalysts. It was found that doping with Cu influenced the catalytic performance of the catalyst. Also, higher Cu contents led to higher glycerol conversions and hydrogen production. Hakim's group came to the conclusion that the interaction between CuO and CeO_2 on the hydroxyapatite support in the GSR reaction enhanced the active sites (more active sites) of the catalysts. Moreover, the presence of ceria facilitated the reduction and increased the dispersion of the copper species on the surface of the catalysts. In terms of Ni content, it was found that it does not enhance significantly the production of H_2. As a matter of fact, it is suggested that since for the catalysts with higher Ni loading there is a greater presence of NiO phase on the surface of the catalysts during preparation and calcination, not all the nickel ions substituted the position of Ca^{2+} in the hydroxyapatite support and some metallic nickel became agglomerated.

Profeti *et al*. [86] studied the catalytic activity of Ni/CeO_2-Al_2O_3 catalysts modified with noble metals (Pt, Ir, Pd and Ru) for the GSR reaction. The addition of noble metals stabilizes the Ni sites in the reduced state, increasing the glycerol conversion and decreasing the coke formation. Moreover, this stabilization of the nickel surface species interacting with the support occurs at lower temperatures in the presence of small amounts of noble metals due to hydrogen spillover effect. A more detailed review on noble metal-based catalysts for GSR is done in further sections.

3.2 Pt-based Catalysts

Noble metal catalysts normally are more active and stable towards the GSR reaction that Ni-based materials [87]. Pt-based catalysts are no exception and because of that, many authors have studied the potential of these catalysts for H_2 production through this process.

3.2.1 Effect of the support on the catalytic performance

Platinum catalysts supported on carbon have been investigated for the GSR either for syngas or hydrogen production [88-90]. A summary of the catalytic performance and

operating conditions of some Pt-based catalysts is presented in Table 3. It has been found that Pt/C supported catalysts present higher stability during GSR than other Pt-based materials making use of different supports (Al_2O_3, ZrO_2, MgO/ZrO_2, and CeO_2/ZrO_2); this is due to the very low formation of C_2-hydrocarbons, which is symptomatic of lower carbon formation on the Pt/C catalyst [88]. Sutar *et al.* [89] attained catalytic results for GSR over a Pt/C sample that are in general comparable to the ones presented in the previous section for some Ni-based catalysts. However, for nickel catalysts those results were obtained at temperatures around 600-700 ℃, while in this case the temperature used was 400 ℃ – Table 3. Simonetti *et al.* [88] reported an even more noticeable superior activity of Pt-based catalysts for the GSR compared to nickel ones.

Although Pt/C supported catalysts present very interesting results at relatively low temperatures, they are more suitable for syngas production. Oxide supports, on the other hand, promote the WGS reaction, thus being more appropriated for hydrogen production with lower CO content [88, 93-96]. Despite this, acid ZrO_2 and Al_2O_3 supports lead to fast deactivation of platinum catalysts mainly due to coke deposition, which results from the promotion of lateral reactions of dehydration, hydrogenolysis, dehydrogenation and condensation [88, 97], as seen for Ni-based catalysts. It has been reported that the acidity of supports decreases in the order $Al_2O_3 > ZrO_2 > SiO_2$ [97, 98]. Therefore, a solution for this deactivation problem includes the use of a support with lower acidity, like SiO_2 [91, 97, 99]. According to Pompeo *et al.* [91, 97], the silica support allows the Pt catalysts to promote mainly dehydrogenation reactions and subsequent cleavage of C-C bonds, thus presenting excellent activity to gaseous products, high H_2 selectivity and remarkable stability over time. It was also observed for Pt/SiO_2 supported catalyst that increasing the Pt content maintains the same active phase (same metal dispersion and average particle size). Therefore, the 2 wt.% Pt catalyst shown in Table 3 presented better performance than the 1 wt.% Pt one. Moreover, a comparison between Pt and Ni catalysts supported on SiO_2 was done at 350 and 450 ℃. At these temperatures the Ni-based catalysts ended up deactivating after a couple of hours, while the Pt-based catalysts presented higher stability; moreover, at 350 ℃ the 2 wt.% Pt catalyst was considerably more stable than the 1 wt.% Pt catalyst (Fig. 13) [91].

A Pt/Y_2O_3 catalyst was tested for GSR by Cui *et al.* [54], having presented high glycerol conversion into gaseous products as well as high hydrogen yield.

3.2.2 Effect of the addition of a promoter on the catalytic performance

Similarly to Ni-based catalysts, the performance of Pt-based catalysts can be enhanced by adding promoters. Table 4 summarizes the effect of different promoters on the GSR catalytic activity of Pt-based catalysts. It has been demonstrated that the heat of CO adsorption on Pt-based catalysts can be decreased by the formation of metal alloys [100, 101]. Simonetti *et al*. [90] came to the conclusion that bimetallic Pt-Re/C catalysts with atomic Pt/Re ratios $\leq$ 1 are 5 times more active to syngas production through GSR than monometallic Pt/C and Pt-Re with a higher Pt/Re ratio (10). The authors suggest that the primary promotional effect of Re is to weaken the interaction between CO and the surface, thus leading to faster turnover of catalytic sites. Kunkes *et al*. [93] added Fe; Cu; Sn; Ir; Co; Ni; Rh; Os; Ru; or Re to Pt supported on C. The addition of Fe; Cu; Sn; Ir; Co; Ni; or Rh had a detrimental or neutral effect on the catalytic activity for all reaction temperatures (275-350 ℃). According to Pompeo *et al*. [91], the fact that the coexistence of Pt and Ni did not improve the catalytic performance suggests that the formation of a bimetallic Pt-Ni phase affects the platinum electronic properties. On the other hand, the addition of Os; Ru; or Re to Pt enhanced the syngas production comparatively to Pt/C, being that Re was the promoter that allowed the best syngas production improvement.

The addition of ceria promoter has been verified as advantageous, but in this case for platinum-based catalysts [88, 92, 97]. As already mentioned, the addition of ceria to a support like alumina reduces its acidity, thereby improving the catalyst stability and H_2 selectivity and reducing the formation of undesirable products and coke deposition. Montini *et al*. [92] verified that the $Pt/CeO_2/Al_2O_3$ catalyst, despite presenting improved performance, still deactivated after 20 h time-on stream (Fig. 14) [92]. This deactivation could be due to coke deposition on the active sites and only marginally due to Pt sintering. Similar behavior, in terms of performance enhancement, has been observed for Pt-based catalysts promoted with basic oxides like La_2O_3 [92] and MgO [88]. However, the La_2O_3 promoted catalyst only deactivated after 50 h time-on-stream, as can be seen in Fig. 14.

On the other hand, Pompeo *et al*. [97] reported the attainment, for a $Pt/Ce_4Zr_1\alpha$ catalyst, of higher H_2 selectivity and glycerol conversion to gaseous products than both $Pt/\gamma-Al_2O_3$ and Pt/ZrO_2 catalyst. The promoted catalyst presented higher average platinum particle size than the other two catalysts. Claus and co-authors [102] suggested that larger particles present a higher number of face atoms of the metal crystallite. Moreover, the adsorption of oxygenated hydrocarbons for posterior C-C cleavage can be

preferably performed at face positions, thus leading to higher hydrogen selectivity. Furthermore, the simultaneous presence of Ce and Zr promotes the WGS reaction, thus enhancing the H_2 selectivity [93].

3.3 Co-based Catalysts

Cobalt catalysts have shown good performance in ethanol reforming for hydrogen production and are proposed as appropriate catalytic systems [103-105]. However they have shown significant deactivation through sintering and surface cobalt deactivation. Even so, many authors have investigated in the last years the catalytic behavior of Co-based materials for GSR [23, 106-109].

3.3.1 Effect of the support on the catalytic performance

The use of alumina as support for Co active phase has been reported [107], having been observed the existence of both strong and weak acid sites on the catalyst surface with an acidic/basic ratio of approximately 5.5. Therefore, expected carbon deposition was verified. Moreover, TPO-TPR and TPR-TPO cycles showed different reactivity of the carbon deposited on the surface of the coked catalyst, meaning that there were at least two types of carbon pools on the surface. One of the pools was reactive in the presence of H_2 while the other was inert to H_2, reacting only in the presence of O_2.

Zhang *et al*. [106] verified that Co/CeO_2 catalyst for GSR originated small concentrations of CH_4 and CO at the reactor outlet stream. Furthermore, only slight changes on their concentrations were observed while increasing the reaction temperature, meaning that the Co/CeO_2 catalyst did not catalyze effectively both WGS and steam reforming of methane. Dehydration of glycerol was not observed over the ceria-supported catalyst, and so no significant deactivation occurred.

A comparison of the catalytic performance of both types of catalysts described along this section for GSR is presented in Table 5.

3.3.2 Effect of the addition of a promoter on the catalytic performance

It has been found that bimetallic $Co-Ni/Al_2O_3$ catalyst, used by Adesina *et al*. [108], presents an enhanced activity for steam reforming of methane and propane due to the

synergism between the Ni and Co metals [110]. The reasons of such synergism are not, however, disclosed. The coexistence of both Lewis and Bronsted acid sites was discovered through physicochemical characterization. However, the bimetallic catalyst presents a net surface acidity (acidic/basic ratio of 9). Analogously to what was reported elsewhere [107], it was verified the occurrence of carbon deposition during reaction, which led to a reduction of the surface area and pore volume of the catalyst. Furthermore two types of carbon deposits were observed once again, being that one of them is inert to H_2 as well. The GSR catalytic activity of this promoted catalyst is compared in Table 5 with that for the non-promoted catalysts presented in the previous section.

CeZr mixed oxides have also been target of attention since they allow the insertion of transition metals, like Co and Ni, and/or noble metals, like Ru and Rh, into the oxide structure, thus increasing the active phase-support interaction [111-113]. Araque *et al*. [23] evaluated the effect of the active phase by using two mixed oxide catalysts: $Ce_2Zr_{1.5}Co_{0.5}O_{8-\delta}$ and $Ce_2Zr_{1.5}Co_{0.47}Rh_{0.07}O_{8-\delta}$. Rhodium did not significantly affect the glycerol total conversion. However, it highly affected the conversion of glycerol into gaseous products at the expense of liquid ones. It was also observed an enhancement of the 24 h average H_2 production from 1.6 $molH_2 \cdot mol_{Gly.in}^{-1}$ up to 5.8 $molH_2 \cdot mol_{Gly.in}^{-1}$ when Rh was added to the mixed oxide catalyst. Also, for the Rh-containing catalyst, an average production of H_2 of 6.7 $molH_2 \cdot mol_{Gly.in}^{-1}$ was obtained for over 16 h, while the other catalyst kept stable only for 1 h. The enhanced behavior of the Rh containing catalyst is related to the capacity of Rh to break the C-C bonds. The loss of activity verified is due to the loss of the C-C bond breaking capacity, since C_2H_4 formation was observed when deactivation occurred. In another work, Roger and co-authors [109] studied the effect of the Ce/Zr ratio in fluorite-type mixed oxides of CeZr-CoRh catalysts on the H_2 production by GSR. Catalysts with three different Ce/Zr ratios were prepared: $Ce_{0.53}Zr_{2.97}Co_{0.47}Rh_{0.03}O_{8-\delta}$ with poor ceria content (CZ^PCoRh), $Ce_2Zr_{1.5}Co_{0.47}Rh_{0.03}O_{8-\delta}$ with intermediate ceria content (CZ^ICoRh), and $Ce_{2.59}Zr_{0.91}Co_{0.47}Rh_{0.03}O_{8-\delta}$ rich in ceria (CZ^RCoRh). It was observed that the increase of the Ce content enhances both the stability (Fig. 15) [109] and selectivity towards H_2 and CO_2. This happens because of the improved cobalt reducibility and re-oxidation properties, oxygen storage capacity and metal support interaction. Also, the catalytic stability and activity of the catalysts is related to their capacity to activate H_2O under reaction conditions, thus favoring the steam reforming reaction over the decomposition reaction. By increasing the Ce content, the H_2O activation is favored for a

longer period of time, thus allowing carbon gasification and delaying the catalyst deactivation; even so this effect is not very pronounced (Fig. 15).

3.4 Ru-based catalysts

Ruthenium is currently, along with nickel and platinum, one of the most promising materials to catalyze hydrogen production through GSR. Moreover, Ru is the least expensive among all noble metals [114]. Ru-based catalysts have been reported has having superior catalytic activity for H_2 production, not only through GSR but also through methane steam reforming, for example [1, 115, 116]. By comparing the GSR activity of catalysts loaded with Group 8-10 metals supported on oxides (Y_2O_3, ZrO_2, CeO_2, La_2O_3, SiO_2, MgO, Al_2O_3), the order Ru $\approx$ Rh > Ni > Ir > Co > Pt > Pd > Fe was found in La_2O_3-supported materials [117]. It has also been reported that the order of the catalytic activity of Group 8-10 metal catalysts over SiO_2 is as follows: Ru $\approx$ Rh > Ni > Ir > Pt $\approx$ Pd $\gg$ Co $\approx$ Fe [117].

3.4.1 Effect of the support on the catalytic performance

Hirai *et al*. [117] prepared several catalysts loaded with Group 8-10 metals supported on Y_2O_3, ZrO_2, CeO_2, La_2O_3, SiO_2, MgO, and Al_2O_3 via a conventional impregnation method. Among all the metals used, Ru was the one that showed the best catalytic activity. Therefore, since ruthenium allowed the attainment of the highest H_2 yield, the effects of the previously mentioned supports for ruthenium on GSR were evaluated at 600 ℃. The Ru/MgO supported catalyst showed very low glycerol conversion to gaseous products compared to the other samples. This low activity is due to the fact that ruthenium on MgO is hard to be reduced to metallic ruthenium and so the number of active sites would decrease [118]. The Ru/Al_2O_3 supported catalyst presented the lowest glycerol conversion into gaseous products. It also showed low H_2 yield because of the higher selectivity towards methane production and lower selectivity to CO_2. On the other hand, both Ru/Y_2O_3 and Ru/ZrO_2 supported catalysts presented high glycerol conversion into gaseous products and H_2 yield. In fact, the Ru/Y_2O_3 sample was the one that presented the best results. This has been attributed to the ability of yttria to promote de WGS reaction [119]. Considering this, an optimization of the loading level of ruthenium was performed at 500 ℃, to compare the catalytic activity at lower conversions [117]. The H_2

yield kept increasing as the ruthenium loading increased up to 3 wt.%. A further increase in the ruthenium loading to 5 wt.% did not affect the H_2 yield and so, the optimal loading was found to be 3 wt.%. Finally, it was observed that both glycerol conversion into gaseous products and H_2 yield did not decrease during a 24 h time-on-stream test, as shown in Fig. 16 [117]. Very small carbon deposition was verified after 24 h reaction, thus meaning that the 3 wt.% Ru/Y_2O_3 material is apparently resistant for the deactivation caused by carbon deposition. However, some deactivation caused by sintering of the dispersed catalytic metal clusters was observed. Ultimately the authors concluded that the Ru/Y_2O_3 catalyst presents very high performance in GSR. The catalytic performance of some of these Ru-based catalysts for GSR is presented in Table 6.

3.4.2 Effect of the addition of a promoter on the catalytic performance

Kim and Lee [119] studied the GSR on Ru and Ru-Me (Me = Fe, Co, Ni, and Mo) catalysts supported on Y_2O_3, $Ce_{0.5}Zr_{0.5}O_2$, and commercial γ-Al_2O_3. It was verified that the use of different supports affects the performance of the catalysts, being that for the Ru-based catalysts supported on reducible yttria and ceria-zirconia there was a significant enhancement of the H_2 production turnover rate and selectivity. This happens because these supports tend to facilitate the WGS reaction. On the other hand, the acidic γ-alumina supported Ru-based catalysts showed low H_2 production turnover rate, high CO selectivity and formation of C_1-C_2 hydrocarbons for the reasons already stated.

In opposition to what was verified for the different supports, the metallic promoters did not influence much neither H_2 production rate nor selectivity. On the other hand, the addition of metallic promoters led to lower catalysts deactivation. In terms of coke deposition, both yttria and ceria-zirconia supports showed superior resistance against coke formation on the catalysts. In fact, very small deposited amounts of carbonaceous species were verified for these supports (< 3 wt.%). However, deactivation of the catalysts at levels between 15% and 80% was observed. Since the low amounts of deposited coke could never lead to such deactivation levels, the authors suggest that sintering of the dispersed catalytic metal clusters was the cause of the verified activity drop. As can be seen in Fig. 17 [119], the $Ru-Mo/Ce_{0.5}Zr_{0.5}O_2$ and $Ru-Mo/Y_2O_3$ catalysts exhibited superior stability against deactivation by sintering and lower carbon deposition. The results suggest that the MoO_x species effectively diminished sintering of the surface metal clusters.

Ru-based catalysts supported on Mg(Al)O mixed oxide were reported by Gallo *et al*. [120, 121]. The Mg(Al)O mixed oxide support plays an important role in enhancing the performance of the catalyst. Ru based catalysts supported on Mg(Al)O mixed oxides have been reported in the literature to present good performance in steam reforming of ethanol [123], acetic acid [124] and hydrocarbons [125-127]. It is known that Mg(Al)O oxides are able to stabilize supported metal nanoparticles, even at high operating temperatures and/or glycerol concentrations, thus avoiding metal nanoparticles sintering [120]. The presence of Mg in the support is, in part, responsible for this good behavior. The effect of Sn doping on the bimetallic Ru-Sn/Mg(Al)O supported catalysts was accessed as well by using catalysts with different Sn loadings [120]. The Ru-based catalyst without tin showed very high glycerol conversion with high selectivity towards H_2 and CO_2, and CO selectivity lower than 10% during the entire catalytic run. By increasing the tin loading, a progressive increase in both CO and CH_4 selectivity was verified. On the other hand, the CO_2 selectivity decreased gradually. Therefore, the catalysts that showed the most attractive results in terms of specific H_2 productivity (mmol H_2·mmol Ru_{exp}^{-1}·min^{-1}) and specific activity (mmol glycerol·mmol Ru_{exp}^{-1}·min^{-1}) was the catalyst with the lowest tin content (Sn/Ru molar ratio of 0.33). It was concluded that the addition of tin has different effects depending on the Sn/Ru molar ratios. For low Sn/Ru molar ratios it was verified that both activity and H_2 productivity per exposed Ru sites are significantly enhanced, since tin selectively coated Ru faces, and only co-ordinatively unsaturated Ru sites, which are the most active ones, are exposed. However, by increasing the ratio a large amount of acidic tin oxides is unselectively deposited onto support materials. Therefore, glycerol decomposition is promoted rather than GSR, thus leading to high amounts of CO and finally to coke deposition responsible for the catalyst deactivation [120]. A comparison between the GSR performance of some of the promoted ruthenium catalysts here discussed and the non-promoted catalysts discussed in the previous section is presented in Table 6.

3.5 Other noble metal-based Catalysts

In addition to the materials analyzed in the previous sections, there are others that have not been so frequently reported in the literature for H_2 production through GSR, but still present some interesting results. In this section some of those materials are reviewed.

Zhang *et al.* [106] studied, has already mentioned, the performance of ceria-supported Ir, Co and Ni catalysts for GSR in the temperature range between 250-600 ºC. Among all the catalysts tested, the Ir/CeO$_2$ sample was the one that presented the best performance. It was verified that the methane concentration greatly decreased with increasing temperature, thus meaning that the steam reforming of methane has occurred in a significant extent. Consequently, most of the produced methane was converted into H$_2$. Also, the increasing concentrations of CO$_2$ in the outlet gas stream and progressively lower CO content for increasing temperatures, indicates that the Ir/CeO$_2$ catalyst successfully catalyzes the WGS reaction. Therefore, Ir/CeO$_2$ seems to be a very promising catalyst for GSR.

Chiodo and co-workers [128] reported the comparison between a Rh/Al$_2$O$_3$ catalyst and several Ni supported materials for the GSR. The group came to the conclusion that the rhodium catalyst is more active and stable than the nickel-based ones. However, after approximately 8 h fast deactivation of the catalyst was verified. Rodhium catalysts are more resistant to coke formation than Ni-based due their high activity in hydrogenation reactions which, in case of removal of unsaturated compounds from the catalyst surface, is fundamental to avoid coke formation. Furthermore, Rh materials are active in C=C bond activation. Considering that the main species that reach the catalyst surface are CO and olefins (C$_2$H$_4$, C$_3$H$_6$), it is therefore deducible that the catalytic performance depends on the tendency towards C=C cleavage and coke formation inhibition through polymerization of CH$_x$ species and/or CO dissociation (Boudouard reaction) [129-132]. Despite this, there are still some improvements that need to be done regarding the relatively fast deactivation of Rh-based catalysts.

Ebshish *et al.* [133] compared the catalytic performance of 1 wt.% Ce/Al$_2$O$_3$ and 1 wt.% Pd/Al$_2$O$_3$ catalysts, as well as the performance of 1 wt.% Ce/Al$_2$O$_3$ and 10 wt.% Ce/Al$_2$O$_3$. The authors observed that the 1 wt.% palladium catalyst supported on alumina presented better glycerol conversion to gaseous products as well as better H$_2$ yield than both 1 wt.% Ce/Al$_2$O$_3$ and 10 wt.% Ce/Al$_2$O$_3$ catalysts. In terms of H$_2$ selectivity, the 10 wt.% Ce/Al$_2$O$_3$ sample was superior to the other two catalysts, having low amounts of carbon oxides been formed. This enhancement was suggested to be due to the higher metal loading. However, it also presented higher carbon formation than the other Ce-based catalyst. It has been concluded that in general Pd is more active and more stable than Ce because of its favorable lattice parameters. It is also important to remark the

fact that this was the first time that Ce was reported as having been used as a catalyst for GSR. In all the previous works, only its oxide had been used as catalyst support.

A summary of some of the catalysts reviewed in this section and their catalytic performances in GSR is presented in Table 7.

4 Mechanisms and Kinetics

Establishment of reaction rate equations for any process, and for GSR in particular, is crucial for reactor design, while the comprehension of the associated mechanism may lead to improvements in catalyst design with the inherent implications at industrial scale. In the last years many authors have studied the kinetics of the GSR over different catalysts and have proposed different reaction mechanisms, being that there has not been full agreement on this matter. In this section a review of the proposed reaction kinetics, as well as the most accepted reaction mechanisms is done. This is, as mentioned above, fundamental for reactor modeling, design, optimization and operation.

Normally the reaction rate data for the GSR have been fitted to a general power-law type equation with the following form:

$$- r_{GSR} = k p_G^a p_W^b \tag{15}$$

where k is the reaction rate constant (defined by the Arrhenius equation), p_G and p_W and a and b are the partial pressures and the reaction orders of glycerol and steam, respectively.

Normally it is difficult to compare activation energies reported in the literature since the conditions used differ from study to study. Moreover, special attention should be put on whether or not mass (and even heat) transfer resistances are absent, so that cases of kinetics falsification can be identified. In Table 8 are presented some literature values of kinetic parameters obtained for some of the most relevant GSR catalysts in the absence of any resistances. In terms of activation energy, a comparison between all the Ni-based and Co-based catalysts presented in Table 8, which were tested at higher temperatures, can however be done. Among these catalysts, it is possible to notice that while the Ni or Co/Al$_2$O$_3$ supported catalysts present activation energies around 60-70 kJ/mol, both the 24.1 wt.% Ni- 26.1 wt.% Mg- 49.8 wt.% Al sample and the 15 wt.% Ni- 10 wt.% ZrO$_2$/CeO$_2$ material present activation energies of 38 kJ·mol^{-1} and 43 kJ·mol^{-1}, respectively. This suggests that the reaction mechanism or the rate-determining step for the last two samples may be different from that over the other catalysts. On the other hand, both Ru-based and Pt-based catalysts were tested at lower temperatures, being that the 5% Ru/Al$_2$O$_3$ sample, among all catalysts in Table 8, is the one that presents the lowest activation energy. Vaidya and co-authors [114] suggest that this might occur due
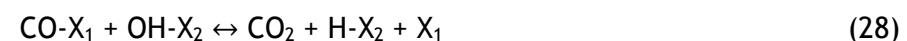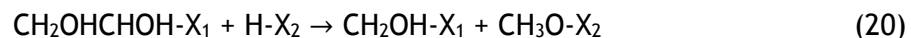
to the enhanced catalyst activity even at low reaction temperatures, which is associated to the high loading level of Ru. It should also be noticed the substantial difference between the activation energies of both Ni/CeO_2 catalysts (36.5 vs. 103.4 kJ·mol^{-1}). Since for both cases, external and internal mass transfer limitations were minimized by selecting suitable flow rates and an appropriate particle size range, respectively, this peculiar difference may be associated to the different temperature ranges used, possibly different metal loadings, and different preparation methods. The last factor is probably the one that contributes the most to the verified significant difference. In comparison to the wet impregnation technique, the deposition-precipitation method improves, among other things, the metallic dispersion and decreases catalyst sintering.

In terms of glycerol partial reaction order, all Ni-based catalysts presented similar values (0.2-0.5) except for the Ni-Mg-Al sample, which presents a value of 1.0. This difference suggests that different reaction mechanisms or different rate-determining steps may exist for these catalysts. Regarding the Co-based materials, both present low values of glycerol partial reaction order, especially the Co/Al_2O_3 catalyst. As a matter of fact, this catalyst also presents small values of glycerol partial reaction order for the production of C_1 products (CO_2, CO and CH_4). This might indicate the existence of a cancellation effect of the molecularly adsorbed glycerol in the rate-controlling step and the presence of a glycerol adsorption term in the denominator of the Langmuir-Hinshelwood rate expression (see eq. (30)) [107]. Therefore, an apparent reduced order for glycerol in the overall reaction rate is obtained. For the Pt- and the Ru-based catalysts, glycerol partial reaction orders of 1 were considered as a valid approach for the low glycerol concentrations used. However, this assumption may not be valid for more concentrated solutions, which can be used during real operation in reformers. In terms of H_2O reaction order, for most of the catalysts in Table 8 it is considered to be zero due to the use of excess of water. For the others, however, values between 0.3-0.4 were obtained despite the excess steam used.

The formation rates of H_2, CO_2, CO and CH_4 have been often fitted to a power-law expression (eq. (15)) as well [107, 108, 134]. For all cases, the formation rate of CO was inhibited by steam (negative value of b). This can either be because of the competitive adsorption of steam on the same active sites as the surface precursor for CO production (especially at high steam partial pressures), or because of CO consumption via WGS reaction [134]. For the other gases, positive values of a and b were obtained, meaning

that both glycerol and steam positively contribute to H_2, CO_2 and CH_4 formation. In terms of activation energy, H_2, CO_2 and CO formation present similar values (in the range 60-75 kJ·mol^{-1}) [108, 134] while the formation of methane presents a much higher activation energy (100-120 kJ·mol^{-1}) [107, 108, 134].
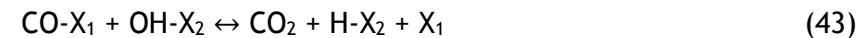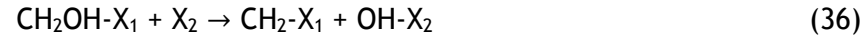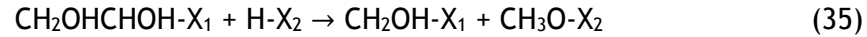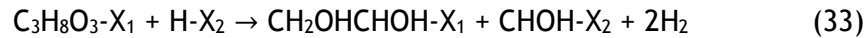
In what concerns the reaction mechanism, Adesina and co-workers [108] came to the conclusion that the most adequate one for the GSR reaction over the 5 wt.% Co-10 wt.% Ni/Al$_2$O$_3$ catalyst is the Langmuir-Hinshelwood dual site mechanism with molecular adsorption of both glycerol and steam. This mechanism involves the following steps:

$$C_3H_8O_3 + X_1 \leftrightarrow C_3H_8O_3\text{-}X_1 \tag{16}$$

$$H_2O + X_2 \leftrightarrow H_2O\text{-}X_2 \tag{17}$$

$$C_3H_8O_3\text{-}X_1 + H_2O\text{-}X_2 \rightarrow HCOO\text{-}X_2 + CH_2OHCHOH\text{-}X_1 + 2H_2 \tag{18}$$

$$HCOO\text{-}X_2 \rightarrow CO_2 + H\text{-}X_2 \tag{19}$$

$$CH_2OHCHOH\text{-}X_1 + H\text{-}X_2 \rightarrow CH_2OH\text{-}X_1 + CH_3O\text{-}X_2 \tag{20}$$

$$CH_2OH\text{-}X_1 + X_2 \rightarrow CH_2\text{-}X_1 + OH\text{-}X_2 \tag{21}$$

$$CH_2\text{-}X_1 + H\text{-}X_2 \rightarrow CH_3\text{-}X_1 + X_2 \tag{22}$$

$$CH_3\text{-}X_1 + H\text{-}X_2 \rightarrow CH_4 + X_1 + X_2 \tag{23}$$

$$CH_3O\text{-}X_1 + X_2 \rightarrow CH_2O\text{-}X_1 + H\text{-}X_2 \tag{24}$$

$$CH_2O\text{-}X_1 + X_2 \rightarrow HCO\text{-}X_1 + H\text{-}X_2 \tag{25}$$

$$HCO\text{-}X_1 + X_2 \rightarrow CO\text{-}X_1 + H\text{-}X_2 \tag{26}$$

$$CO\text{-}X_1 \leftrightarrow CO + X_1 \tag{27}$$

$$CO\text{-}X_1 + OH\text{-}X_2 \leftrightarrow CO_2 + H\text{-}X_2 + X_1 \tag{28}$$

$$2H\text{-}X_2 \leftrightarrow H_2 + 2X_2 \tag{29}$$

where X_1 and X_2 represent the basic and the acid active sites, respectively. The authors suggested that surface reaction was rate-controlling, and so the following kinetic expression was proposed [108]:

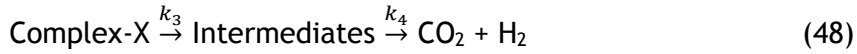$$r = \frac{k p_G p_W}{(1+ K_G p_G)(1+ K_W p_W)} \qquad (30)$$

where K_G and K_W are the adsorption constants of glycerol and steam, respectively. In another work, Cheng et $al.$ [134] concluded that the GSR reaction rate over a Ni/Al_2O_3 supported catalyst is better described by a Langmuir-Hinshelwood model considering molecular adsorption of glycerol and dissociative chemisorption of steam, on two different sites, with the surface reaction as rate-determining step. The authors proposed the following mechanism represented by eq. (31-44).

$$C_3H_8O_3 + X_1 \leftrightarrow C_3H_8O_3\text{-}X_1 \qquad (31)$$

$$H_2O + 2X_2 \leftrightarrow OH\text{-}X_2 + H\text{-}X_2 \qquad (32)$$

$$C_3H_8O_3\text{-}X_1 + H\text{-}X_2 \rightarrow CH_2OHCHOH\text{-}X_1 + CHOH\text{-}X_2 + 2H_2 \qquad (33)$$

$$CHOH\text{-}X_2 \rightarrow CO\text{-}X_2 + H_2 \qquad (34)$$

$$CH_2OHCHOH\text{-}X_1 + H\text{-}X_2 \rightarrow CH_2OH\text{-}X_1 + CH_3O\text{-}X_2 \qquad (35)$$

$$CH_2OH\text{-}X_1 + X_2 \rightarrow CH_2\text{-}X_1 + OH\text{-}X_2 \qquad (36)$$

$$CH_2\text{-}X_1 + H\text{-}X_2 \rightarrow CH3\text{-}X_1 + X_2 \qquad (37)$$

$$CH_3\text{-}X_1 + H\text{-}X_2 \rightarrow CH_4\text{-}X_1 + X_2 \qquad (38)$$

$$CH_3O\text{-}X_1 + X_2 \rightarrow CH_2O\text{-}X_1 + H\text{-}X_2 \qquad (39)$$

$$CH_2O\text{-}X_1 + X_2 \rightarrow HCO\text{-}X_1 + H\text{-}X_2 \qquad (40)$$

$$HCO\text{-}X_1 + X_2 \rightarrow CO\text{-}X_1 + H\text{-}X_2 \qquad (41)$$

$$CO\text{-}X_1 \leftrightarrow CO + X_1 \qquad (42)$$

$$CO\text{-}X_1 + OH\text{-}X_2 \leftrightarrow CO_2 + H\text{-}X_2 + X_1 \qquad (43)$$

$$H\text{-}X_2 + H\text{-}X_2 \leftrightarrow H_2 + 2X_2 \qquad (44)$$

This mechanism yielded the following rate equation [134]:

$$r = \frac{kP_G\sqrt{P_W}}{(1+K_GP_G)(1+\sqrt{K_WP_W})} \tag{45}$$

In another mechanistic study, Byrd *et al.* [15] observed the presence of very low concentrations of organic carbon in the product stream, which suggests that intermediates like alcohols or organic acids, formed from C-O cleavage, were further transformed into gaseous products. For this reason, a different mechanism was proposed to describe the GSR over the 5% Ru/Al$_2$O$_3$ catalyst [114] and was also admitted to be valid for the 15 wt.% Ni/CeO$_2$ one [50]. This mechanism involves the reversible adsorption of glycerol on the catalyst active sites followed by its reaction with water, thus forming an adsorbed complex molecule. This complex on its hand decomposes into intermediate products, which irreversibly yield H$_2$ and CO$_2$. These steps are described by the following equations:

$$C_3H_8O_3 + X \xrightarrow{k_1,k_{-1}} C_3H_8O_3\text{-}X \tag{46}$$

$$C_3H_8O_3\text{-}X + H_2O \xrightarrow{k_2} \text{Complex-X} \tag{47}$$

$$\text{Complex-X} \xrightarrow{k_3} \text{Intermediates} \xrightarrow{k_4} CO_2 + H_2 \tag{48}$$

By applying steady state hypothesis to C$_3$H$_8$O$_3$-X and Complex-X and assuming that the decomposition of Complex-X into intermediate products is the rate-determining step, the reaction rate was expressed as [50, 114]:

$$r = \frac{k_1k_2p_Gp_W}{[k_{-1}+k_1p_G+k_2p_W+(k_1k_2p_Gp_W/k_3)]} \tag{49}$$

Considering that water is in excess and that the operation pressure is constant, p_W can be assumed to be almost equal to p_{W0}. Therefore, eq. (49) is simplified to:

$$r = \frac{kp_G}{1+bp_G} \tag{50}$$

where k and b are defined as:

$$k = \frac{k_1k_2p_{W0}}{k_{-1}+k_2p_{W0}} \tag{51}$$

$$b = \frac{k_1+(k_1k_2p_{W0}/k_3)}{k_{-1}+k_2p_{W0}} \tag{52}$$

Carbon deposition, as already discussed, is one of the most common causes of catalyst deactivation in GSR reaction. The influence of carbon deposition on the physical properties of the catalyst has already been discussed, as well as the nature of these deposits. On the other hand, the determination of carbon deposition kinetics is very helpful in terms of creation of more realistic reactor models, and better reactor design and operation. Cheng *et al*. [136] observed that the coke deposition rate on a 5 wt.% Co-10 wt.% Ni/Al$_2$O$_3$ catalyst during GSR can be relatively well described by a power-law model as follows:

$$r_{coke\ deposition} = k_C p_G^a p_W^b \qquad (53)$$

where k_C is the coke deposition reaction rate constant. At temperatures between 500-550 °C and glycerol partial pressures between 4.5-16.5 kPa, the parameters a and b were determined to be 0.55 and -0.22, respectively, being the activation energy 40.9 kJ·mol^{-1}. These values were found to be lower than those obtained for carbon deposition caused by C$_3$H$_8$ [137, 138], which is structurally very similar to glycerol. Regarding the lower activation energy, it may be explained by the presence of the functional OH group on each of the carbon atoms in the parent chain of glycerol, which makes it more reactive than propane (less electron-withdrawing H on each C atom). Moreover, the equilibrium constant of propane dehydrogenation into hydrogen and carbon is lower than that of glycerol decomposition into carbon. Therefore, the authors concluded that the adsorption of glycerol is stronger than for propane, in other words, it leads to easier carbon deposition [136]. Keeping this in mind and considering the empirical rate law, it was suggested that glycerol adsorbs dissociatively while steam is molecularly chemisorbed. Therefore, a Langmuir-Hinshelwood rate model considering a bimolecular rate-controlling step was proposed [136], yielding the following rate equation for coke deposition.

$$r_{coke\ deposition} = \frac{k_C p_W \sqrt{p_G}}{\left(1 + K_W P_W + \sqrt{K_G p_G}\right)^2} \qquad (54)$$

5 Sorption-Enhanced Reactors

In the last years, alternatives for improving the catalytic GSR process have been investigated. The main common reason that motivates this search is the necessity of overcoming equilibrium limitations, and also producing highly pure hydrogen that is suitable to be used in PEMFCs, for example. One of those alternatives is the Sorption Enhanced GSR (SEGSR) process, which consists on combining the catalytic GSR and CO_2 capture in the same physical device. This innovative configuration allows "affecting" the thermodynamic equilibrium of the GSR reaction by removing one of the reaction products from the reaction medium. Some of the more important advantages of sorption-enhanced reactors (SER) comparatively to tradition reactors (TR) are:

- Shift the equilibrium of reversible reactions towards higher conversions;
- Enhancement of both hydrogen yield and selectivity;
- Attainment of better performance than in a TR at the same (or even less drastic) operating conditions.

However, the main disadvantage of this system is that the CO_2 sorbent gets saturated at some point and then regeneration is necessary. In order to be possible to run continuously, the system must encompass, for example, two reactors, being that while one of them is used as SER the other is used as regenerator; the approach is the same as used in other cyclic processes like PSA (Pressure Swing Adsorption), etc. Another example of such a continuous SEGSR system is presented in Fig. 18 [139]. Besides the two moving-bed reactors in which both catalyst and sorbent are moved at a velocity of 9-11 cm·min^{-1}, a riser is used for transporting the particles with N_2. There is also a system for injecting the particles of catalyst and sorbent at the top of the reactor (cyclone section) in order to compensate for the losses during the runs, which amount is close to 5% every 5 min [139].

The successful use of SERs for GSR depends, above all, on choosing an adsorbent with suitable characteristics and selecting appropriate operating conditions. Such matters are target of focus in the following section.

5.1 CO$_2$ Sorbents

Different materials like hydrotalcites [140-144], CaO-based materials [145-149], lithium zirconates [150-154] and lithium silicates [155-159], among others, have been

reported in the literature as CO_2 sorbents for SERs applications. It is expected from a good CO_2 sorbent to couple in a GSR process to present high CO_2 capture capacity and selectivity at moderated temperatures (300-500 °C), good regenerability (adequate sorption-desorption kinetics), good hydrothermal and mechanical stability and low-cost [160-163]. The sorption capacities and sorption/regeneration temperatures of several sorbents are summarized is Table 9.

Hydrotalcites are a family of clay minerals that consist of a double-layered hydroxide structure with the general formula $[M^{II}_x M^{III}_{(1-x)}(OH)_2][A^{n-}]_{x/n} \cdot m H_2 O$, where M^{II} and M^{III} represent di- and trivalent metal ions inside the brucite-like layers and A^{n-} is a charge compensating anion [143, 167]. Aschenbrenner *et al*. [143] observed that NiMgAl hydrotalcite presented 53% more adsorption capacity than NiMgAlFe hydrotalcite and high stability. A comparison between a commercial hydrotalcite and two potassium and potassium-sodium containing hydrotalcites allowed to conclude that the last one presented the highest adsorption capacity while the potassium containing hydrotalcite presented no significative deactivation after more than 50 cycles of operation [142]. K-doped hydrotalcite-based sorbents have been reported elsewhere to present a CO_2 capture capacity as high as 9 mol·kg^{-1} at 300 °C but under wet conditions (Table 9) [141]. Under dry conditions, the maximum value reported was around 1.8 mol·kg^{-1} (Table 9), which is an outstanding value taken into account the temperature (300 °C) and that it was not tested under the presence of steam. It has also been found that the physical and chemical properties of hydrotalcites are highly influenced by the charge compensating anion used. Wang *et al*. [168] analyzed several charge compensating anions (CO_3^{2-}; HCO_3^-; NO_3^-; SO_4^{2-}; and Cl^-) having observed that when using CO_3^{2-}, a spheroidal "sand rose" type of hydrotalcite with very high BET surface area (114.3 m^2·g^{-1}) was produced. On the other hand, the other anions led to the formation of "stone" type hydrotalcites with very low surface areas (<9 m^2·g^{-1}). For this reason, the Mg_3Al_1-CO_3 hydrotalcite presented the highest CO_2 capture capacity. The thermal stability was also found to depend on the anion used, being that the Mg_3Al_1-SO_4 was the one that presented the highest thermal stability.

Other adsorbents like CaO-based materials, and lithium zirconates and silicates present in general a lower CO_2 capacity and slower adsorption kinetics at 300-400 °C, higher regeneration temperature (>650 °C) and gradual deactivation due to sintering of the active surface [140]. They have however significant adsorption capacities, but at much higher temperatures (Table 9). Wang *et al*. [145] avoided sintering of nano $CaCO_3$ during

31

multiple carbonation/calcination cycles by applying a TiO_2 coating. Akgsornpeak *et al.* [149] avoided the same problem by preparing CaO sorbents through sol-gel synthesis in the presence of cetyltrimethyl ammonium bromide (CTAB). Besides that, the CaO sorbents prepared with CTAB also exhibited high carbonation reaction rates, and the best CaO sorbent presented carbonation conversion 154% more effective than the CaO prepared in the absence of CTAB. The incorporation of Y_2O_3 has been recently reported to significantly enhance the carbonation rate and adsorption capacity of CaO-based CO_2 sorbents [147]. Similarly to hydrotalcites, the addition of optimized amounts of K to Li_2ZrO_3 sorbents was reported to enhance its CO_2 sorption rate and capacity. Moreover, they showed good stability [152]. However, Lapkin and co-workers [154] came to the conclusion that a traditional route to K-doped materials result in slow regeneration. On the other hand, a new soft chemistry route that produces high surface area undoped materials led to much higher rates of reaction/regeneration. Seggiani *et al.* [156] analyzed the performance of different doped-Li_4SO_4 CO_2 sorbents, having observed that the K-doped and Na-doped presented the highest CO_2 sorption capacities and sorption rates. In terms of stability, only the potassium-doped sorbent was able to keep its properties after 25 sorption/desorption cycles. In another work, it was shown that Li_4SiO_4 treated with glacial acetic acid presented stable CO_2 sorption capacity, higher specific surface area and higher porosity than limestone and Li_4SiO_4 without acid treatment [157].

The decision on which kind of CO_2 sorbent is more adequate to be used in SEGSR strongly depends on the operating temperature at which it will be employed. Since one of the main goals at the moment is to reduce the GSR temperature in order to reduce operation costs, it is desirable to work at relatively low temperatures (300-500 ℃). For such temperatures hydrotalcites have been reported to present higher CO_2 capacities and faster sorption kinetics, as well as easier regeneration, and lower loss of sorption capacity [140, 141]. Moreover, the fact that the CO_2 capacity of hydrotalcites is strongly enhanced under wet conditions (steam reforming conditions) makes them an even better candidate for use in SEGSR.

5.2 Sorption Enhanced Glycerol Steam Reforming

The catalytic GSR performed in TRs presents some limitations as already mentioned, including the thermodynamic constrains. On the other hand, when CO_2 capture

is performed simultaneously with the GSR reaction in a SER, the thermodynamic equilibrium is shifted towards higher glycerol conversions and hydrogen yields. A typical evolution profile of the product gas composition (N_2 free and dry basis) in a SEGSR over a mixture of Ni-Co/hydrotalcite-like catalyst and calcined dolomite as CO_2 sorbent is illustrated in Fig. 19 [169]. The performance of the SEGSR is highly dependent on the CO_2 capture. It can be seen in Fig. 19 that there are 3 distinct regimes along time: pre-breakthrough, breakthrough and post-breakthrough. In the pre-breakthrough regime (up to 140 min), most of the CO_2 was removed by fast carbonation reaction with CaO, thus enhancing hydrogen production. In the breakthrough regime the H_2 concentration starts decreasing. In the post-breakthrough regime the CaO sorbent is already saturated and so the enhancement of hydrogen production due to CO_2 removal disappears; at this stage the SEGSR becomes GSR (conventional fixed-bed reactor).

In the following sections are shown the effects of the main operating conditions in the SEGSR, comparing, whenever possible, with the thermodynamic equilibrium.

5.2.1 Effect of Temperature

The influence of temperature on the performance of a SEGSR reactor has been analyzed by several authors, due to the crucial importance of choosing an appropriate temperature range in order to fully benefit of the advantages of this innovative reaction-separation system.

Chen *et al*. [44] compared the product gas composition of a GSR reactor obtained with and without in situ CO_2 removal, and each of them with the respective thermodynamic equilibrium limits. Such comparison is depicted in Fig. 20 [44]. The SEGSR tests were performed until the calcined dolomite was saturated, being that from that point on the GSR took place. A Co-Ni/hydrotalcite-like catalyst and ARCTIC dolomite (98.5% $CaMg(CO_3)_2$) CO_2 sorbent were used. Regarding the GSR product gas composition, the thermodynamic equilibrium trends are in general followed by CO and CH_4. However, the H_2 content is slightly higher and the CO_2 content is slightly lower than the equilibrium values for GSR. The authors suggested that this happened because of the very slow CO_2 removal by the dolomite sample in the second carbonation regime (i.e. the reactor was not yet operating as a conventional GSR one, because some carbon dioxide sorption was still occurring). By comparing both SEGSR and GSR it is observed, as expected, that the in

situ selective removal of CO_2 enhanced the hydrogen production and originated a lower CO content due to the promotion/shift of the WGS reaction equilibrium, which consequently promoted SRM. Both experimental and thermodynamic equilibrium gas composition values are in agreement for SEGSR. In terms of the effect of temperature, a compromise between the WGS reaction, SRM and CO_2 sorption has to be considered. At higher temperatures, both exothermic WGS reaction and CO_2 sorption are less favored while the endothermic SRM is benefited. As can be seen for SEGSR, both CO and CO_2 contents increase with temperature, being that CO is more influenced because of both the increase of CO_2 concentration in the adsorption equilibrium and decrease of the WGS reaction equilibrium constant. The methane content, on the other hand, decreased since high temperatures favor SRM. Finally, the hydrogen purity decreased as well due to the presence of higher amounts of CO and CO_2.

Dou *et al*. [122, 170] analyzed the purity of hydrogen as a function of time at distinct temperatures (400-700 °C [122] and 500-700°C [170]) while using dolomite as CO_2 sorbent. As expected, the highest hydrogen purity was obtained in the pre-CO_2 breakthrough period. The periods of production of hydrogen with purity higher than 90% were 3.6, 6.8 and 5 min at 400, 500 and 600 °C, respectively. At 700 °C, the maximum H_2 purity was 77% with a CO_2 breakthrough time of 0.7 min [122]. A similar behavior was observed in [170]. The authors suggest that the effect of SEGSR was particularly low at 700 °C because the carbonate decomposition (calcination) in the presence of steam is significantly active at that temperature for dolomite. Moreover, the calcined dolomite presents some affinity towards steam in order to form $Ca(OH)_2$ (eq. (13)). In another work, Dou and co-workers [139] observed that the high-purity hydrogen production period did not vary much when the operation temperature was increased from 500 °C to 600 °C, while using CaO as CO_2 sorbent. Chen *et al*. [171] observed, while using an hydrotalcite CO_2 sorbent, a decrease of the GSR enhancement when the temperature was increased from 400 to 500 °C. Thus, the operating temperature should be chosen so that the GSR enhancement caused by in situ CO_2 capture is maximized.

5.2.2   Effect of the Water/Glycerol Feed Ratio

It is well known that the WGFR has an important influence on the GSR reaction. It was verified in section 2.2 that increasing the WGFR affects the thermodynamic

equilibrium of the SEGSR process. However, in actual operation additional effects may occur. Such effects are target of discussion here.

Chen and co-workers [44] analyzed the performance of the SEGSR for different values of WGFR in the range of 3-9. A comparison between the evolution of product composition with time on stream at WGFRs of 3, 4 and 9 was done. During the pre-CO_2 breakthrough period, in particular, the authors observed that for a WGFR of 9 the maximum H_2 purity is higher than that for a WGFR of 3. Moreover, at the lower WGFR the H_2 purity decreased with time on stream. This decay was caused exclusively by the gradual increase of the methane content, since both CO_2 and CO content remained almost constant and low. The authors suggested that the relatively high methane content was not exclusively due to methanation reaction, since only low amounts of CO_2 and CO were present in the gas phase and in the catalyst surface. Thus, considering that SEGSR was performed at high temperatures and glycerol is thermally unstable, the pyrolysis of glycerol to yield CH_4, CO_2, H_2O, coke and volatiles may have happened even before glycerol reached or passed through the catalyst bed. Therefore, pyrolysis of glycerol may have occurred and caused the carbonaceous deposits that were found on the front of the reactor bed and that led to catalyst deactivation. At a WGFR of 4 the purity of H_2 was lower than that for a WGFR of 9, however gradual decrease of the H_2 content due to methane formation through glycerol pyrolysis was not observed at such water content as compared to WGFR of 3.

A comparison between the H_2 yields obtained experimentally and in the thermodynamic equilibrium at different WGFRs was also done by Chen et al. [44]. The biggest difference was obtained for a WGFR of 3. This happened because of the pyrolysis of glycerol that hindered hydrogen production by favoring the formation of CH_4, CO_2 and carbon deposits. As the WGFR increased, the experimental H_2 yield went close to the thermodynamic boundaries, being that at a WGFR of 9 the experimental H_2 yield achieved the theoretical maximum value. In another work, Chen *et al*. [169] obtained lower H_2 yields than in [44] using the same WGFR of 9 but at 550 °C. They suggested that this lower performance was associated to the formation of carbonaceous deposits through glycerol pyrolysis. The reason for such difference is that while in [44] pure glycerol was used, in [169] Chen's group used crude glycerol, whose impurities lead to pyrolysis, thus enhancing coke formation.

Wang *et al*. [172] analyzed the impact of changing the WGFR from 6 to 9 on the product composition (dry basis) of SEGSR. While for a WGFR of 6 a dry product composition

of 87% H_2, 9% CH_4, 3% CO and 1% CO_2 was attained, for a WGFR of 9 a dry product composition of 95% H_2 and 5% of CH_4 was reached. This is due to the enhancement of GSR performance at higher WGFRs. Even though the H_2 concentrations obtained for both cases were high, they were still below the thermodynamic values. Methane concentrations, on the other hand, were higher than the thermodynamic values, which the authors suggested to be due to lack of activity to convert excess methane into hydrogen with the Ni/ZrO_2 catalyst used.

On the other hand, the steam content has been reported to influence the capacity of CO_2 sorbents [141, 142]. By comparing the adsorption capacity of hydrotalcite-based sorbents under dry and wet conditions, Martunus *et al*. [142] and Maroño *et al*. [141] concluded that under wet conditions the CO_2 capture capacities of the sorbents were higher. Dou *et al*. [170] compared the performance of SEGSR using crude glycerol and pure glycerol in the same conditions, having come to the conclusion that when crude glycerol was used longer breakthrough times were observed. This might be explained by the fact that steam conversions obtained while using crude glycerol were approximately half of those obtained for pure glycerol, thus resulting in higher steam partial pressures in the reactor when crude glycerol was used. However, excessive amounts of steam may lead to reduction of CO_2 capture capacity of sorbents, since it causes shrinkage of pore mouths due to adsorption of both steam and CO_2 on the active sorbent surfaces, especially near the pore mouth. Consequently, the pores may be closed, thus increasing the diffusional resistance [142].

5.2.3 Effect of Pressure

It was discussed in section 2 that, in equilibrium, lower pressures favor the production of hydrogen through both GSR and SEGSR and lead to low carbon formation, especially for SEGSR. Chen and co-workers [171] observed that by increasing the operation pressure, the hydrogen yield decreased for both GSR and SEGSR (Fig. 21 [171]). However, as expected, higher values of hydrogen yield were obtained in SEGSR for all pressure range. Moreover, it was observed that the difference between the values of H_2 yield in GSR and SEGSR increased with pressure, as can be seen in Fig. 21. This happens because higher pressures favor CO_2 sorption. Therefore higher pressures allow taking more advantage of the benefits of the SEGSR process.

6 Membrane Reactors

The International Union of Pure and Applied Chemistry (IUPAC) defined MR as a device for simultaneously carrying out a reaction and a membrane-based separation in the same physical enclosure [173]. In a MR the membrane not only selectively separates one or more components but also plays a crucial role, e.g. in overcoming the thermodynamic boundaries of equilibrium-limited reactions like the GSR. Regarding its advantages compared to TRs, they are basically the same as SERs, with exception to the reduction of CO_2 emissions, being that the capital costs reduction is even higher in the case of MRs since only one reactor is needed instead of two reactors. In fact, this cost reduction is feasible as long as cheap and long-lasting membranes can be produced. Moreover, in MRs it is possible to produce ultra-pure hydrogen streams. The scheme of a MR for GSR is presented in Fig. 22 [174]. In this particular case, a hydrogen perm-selective membrane is used to selectively separate hydrogen from the other components; however, a CO_2 perm-selective membrane could be used instead. Still, since one of the main goals of using MRs for GSR reaction is to produce ultra-pure hydrogen that can later be used in PEMFCs, it is preferable to use a H_2 perm-selective membrane in order to isolate H_2 instead of using CO_2 perm-selective membranes and having H_2 mixed with steam, some unreacted CO and glycerol.

In order to fully use all the capacities of MRs, it is fundamental that an appropriate hydrogen perm-selective membrane is used and that the right operating conditions are selected. Therefore, the following sections comprise a short overview on hydrogen perm-selective membranes reported in the literature as well as an analysis of experimental parametric studies on GSR in MRs.

6.1 Hydrogen perm-selective membranes for membrane reactors

Hydrogen perm-selective membranes may be classified as dense metallic membranes (palladium and palladium alloys), proton conducting dense ceramic membranes (perovskites like $SrCeO_{3-\delta}$ and $BaCeO_{3-\delta}$), dense polymeric membranes (polyimide, cellulose acetate, polysulfone, etc), microporous ceramic membranes (silica, alumina, zirconia, titania, zeolites, metal-organic frameworks (MOF)) and porous carbon

membranes (carbon) [175, 176]. The main advantage of dense metallic membranes is that usually they withstand high temperatures (e.g. as compared to polymeric ones) and present higher selectivity towards H_2, thus being possible to obtain high purity hydrogen-permeate streams [175]. Therefore, dense metallic membranes are preferable for ultra-pure hydrogen production and will be the main target of focus.

When choosing a membrane to be used in a MR, one has to consider the operating conditions under which the membrane will be used. In the last years there has been a tremendous effort in order to find suitable membranes for MR applications. Palladium-based membranes are currently the most promising for high purity hydrogen production in MRs, especially palladium alloys (e.g. Pd-Ag and Pd-Cu) which are less sensitive than pure Pd to embrittlement (caused by the presence of H_2 at temperatures below 300 °C and pressures below 2 MPa) and poisoning (caused by contact with CO or H_2S - present in crude glycerol) [175, 177]. Tosti *et al.* [178] verified that self-supported dense Pd-Ag 23 wt.% tubular membranes with finger-type configuration are highly durable and reliable since they allowed to attain complete hydrogen selectivity and no failures were observed after at least one year of thermal and hydrogenation cycles. These characteristics, together with high permeability, make such materials very promising for ultra-pure hydrogen production in industrial and energetic applications (chemical industry, PEMFCs, etc.) [178]. However, the cost of these dense membranes is still a limiting factor, reason why a strong effort has been put in the preparation of thinner Pd films over different supports, by several techniques.

In terms of preparation methods, electroless plating (EP) and chemical vapor deposition (CVD) are the most used ones. The EP method normally consists on producing Pd particles through reduction of a plating solution containing Pd-amine complexes. This technique allows to attain high coating adhesion, involves low operation costs and allows simple operation. However, the impurities present in the plating solution may lead to the presence of defects on the palladium layer deposited on the support. The CVD technique allows to very easily deposit a metal film on a support. On the other hand, using both of these techniques it may be difficult to control the metal alloy composition [179].

Usually the permeation of hydrogen through a palladium-based membrane is described by a solution-diffusion mechanism, being that the flux of hydrogen that permeates through the membrane (J_{H_2}) can be illustrated by the following equation:

$$J_{H_2} = {P_{Pd,H_2}}/{\delta} \left(p^x_{H_2,retentate} - p^x_{H_2,permeate}\right) \qquad (55)$$

where P_{Pd,H_2} is the permeability of the membrane, δ is the membrane thickness, $p_{H_2,retentate}$ and $p_{H_2,permeate}$ are the partial pressures of hydrogen in the retentate and in the permeate side, respectively, and x is the pressure exponent. The ratio $\frac{P_{Pd,H_2}}{\delta}$ is normally called permeance or pressure normalized flux. The pressure exponent takes values between 0.5 and 1, being 0.5 (Sieverts law) when the diffusion of atomic hydrogen through the metal lattice of the membrane is the limiting step. On the other hand, the pressure exponent becomes close to 1 if the surface adsorption is rate limiting. The permeability is typically described by an Arrhenius-type dependency on the temperature:

$$P_{Pd,H_2} = P^0_{Pd,H_2} exp\left(-{E_{a,Pd}}/{RT}\right) \qquad (56)$$

where P^0_{Pd,H_2} is the pre-exponential factor and $E_{a,Pd}$ is the activation energy of the membrane.

Table 10 encompasses a summary of different Pd-based membranes that have been reported in the last years. Some parameters such as membrane thickness, hydrogen permeance, ideal H_2/N_2 selectivity and activation energy are reported.

6.2 Glycerol Steam Reforming in Membrane Reactors

Experimental studies featuring the use of MRs for hydrogen production through several reactions (GSR, SRM, WGS, steam reforming of ethanol, etc.) have been extensively reported in the last decade. This growing interest in such technology is explained by the fact that, among other things, MRs allow to overcome the thermodynamic boundaries of equilibrium-limited reactions, thus allowing to reach high purity hydrogen streams that are suitable for use in PEMFCs. The experimental studies on GSR in MRs reported in the literature [190-193] accessed the effects of temperature, pressure and weight hourly space velocity (WHSV) and will be summarized in the next section.

6.2.1 Effects of Temperature, Pressure and Weight Hourly Space Velocity

In a MR, it was observed that, by increasing the operating temperature from 400 °C to 450 °C, both glycerol conversion and hydrogen yield increased [190, 192]. This

happens not only because of the endothermic nature of the GSR reaction, but also because at higher temperatures the Pd-Ag/PSS membrane becomes more permeable towards hydrogen (eq. (56)). Such enhancement in the performance was also proved by the observed increase in the hydrogen recovery (ratio between the amount of hydrogen collected in the permeate side and the total amount of hydrogen produced in the GSR reaction) when temperature was increased from 400 °C to 450 °C [190]. This way, a higher shift of the thermodynamic equilibrium at higher temperatures is observed.

When it comes to the successful operation of a MR, pressure is a fundamental parameter to be taken into consideration. As can be seen by analyzing eq. (55), higher differences between the retentate and permeate pressures (driving force) lead to higher permeating hydrogen fluxes. Therefore, higher driving forces favor the dislocation of the thermodynamic constraints (Fig. 23 [193]). On the other hand, the production of hydrogen through GSR reaction is not favored at higher pressures, as already discussed in previous sections and illustrated in the same figure. Thus, a compromise between these two factors must be taken into consideration, being, for the conditions employed in Fig. 23, the hydrogen permeation through the membrane the dominant one.

In terms of glycerol conversion, a clear increase was verified with the increase of pressure in several works with MRs [190, 192, 193]. However, Iulianelli *et al*. [191] observed a high increase of glycerol conversion from 1.0 to 4.0 bar and a small decrease from 1.0 to 1.5 bar (Fig. 24 [191]). The authors suggested that this happens because while for the first case the enhancement of the hydrogen permeation prevails over the thermodynamic restrictions, for the second case the opposite occurs. Regarding the hydrogen yield, it increased less and, at higher pressures, it was observed that it stabilized or even decreased. This happens due to the occurrence of methanation reactions which consume hydrogen. Basile and co-workers [191] observed an increase of the methane selectivity as well as a decrease of hydrogen selectivity for increasing pressures. Such behavior is also due to the low capacity of the used Co-based catalyst to promote SRM [191]. Contrarily, the recovery of hydrogen increased even more rapidly at higher reaction pressures.

The use of an inert sweep gas to dilute the hydrogen in the permeate side and decrease its partial pressure has been one of the best ways of increasing the driving force for hydrogen permeation in MRs. Iulianelli *et al*. [191] analyzed the effect of the sweep factor (SF) (molar ratio between the sweep gas and the feed glycerol flow rates) on

glycerol conversion and hydrogen recovery at different reaction pressures. By increasing the SF from 2.6 to 11.9 at 4.0 bar, the glycerol conversion increased from 55.0 to 92.0% (Fig. 24). However, for increasing SFs beyond 11.9 the enhancement of the glycerol conversion is very low. This happens because from a SF of 11.9 on, the increase in the dilution of the hydrogen in the permeate side is almost null and so the driving force almost does not increase. In terms of hydrogen recovery, the best result was around 63.0% and was obtained at 4.0 bar and SF of 22.8.

The effect of the WHSV has also been analyzed by Iulianelli *et al*. [193]. The authors observed that increasing WHSV have a negative impact on the glycerol conversion and on both hydrogen yield and recovery. The lower the WHSV, the higher is the residence time of gases inside the reactor bed and so higher glycerol conversions and hydrogen yields are obtained. Higher residence times also allow hydrogen to permeate more easily, not only because of the higher amounts of hydrogen produced and thus higher driving force, but also because hydrogen has more time to reach the membrane surface and permeate.

Besides affecting the performance of the GSR catalyst, the deposition of carbonaceous deposits was also found to negatively affect the performance of the membrane in terms of hydrogen permeating flux [191]. Moreover, the presence of CO during GSR reaction is often responsible for the loss of membranes permeability, being far more important than CO_2 [177]. One way of reducing this effect is to use higher WGFRs (e.g. 9).

7 Conclusions

In the last decades hydrogen has been seen as a promising energy carrier to be used in energy systems. For this reason, different ways of producing hydrogen have been target of interest. However, most of these processes are based on the use of fossil origin raw materials (natural gas, naphtha, coal, etc.) whose environmental sustainability is highly questionable.

Glycerol produced as by-product in the biodiesel manufacturing process has been found to be a very attractive non-fossil alternative for hydrogen production. The GSR process is seen as one of the most promising ways of converting glycerol into hydrogen, mainly because its scale-up would not require many changes in the current industrial processes for hydrogen production from fossil fuels, which are mostly based on steam reforming. In order to enhance the GSR process performance for improved hydrogen production the choice of an appropriate catalyst is fundamental. Nickel and noble metals like platinum and ruthenium have been widely studied. While nickel catalysts are cheaper, noble metals are more active and stable, thus allowing to work at lower temperatures. Nonetheless, in the last years a huge effort has been put on the search for nickel-based catalysts whose performance is comparable to that of noble metal materials. The influence of catalyst supports must also be taken into consideration, being that neutral supports (e.g. SiO_2) present higher stability and lower carbon deposition. The use of promoters may also be necessary in order to further improve the catalyst stability, a key issue in this field. Consequently, further research has to be done on this area, especially the search for low-temperature active and stable Ni-based catalysts.

Different mechanisms have been proposed for the GSR reaction (e.g. Langmuir-Hinshelwood dual site mechanism with molecular adsorption of glycerol and molecular or dissociative adsorption of water). However, a consensus on this matter hasn't been reached yet and so further studies are required. Moreover, since the GSR reaction highly promotes the formation of carbonaceous deposits, the study of the coke deposition kinetics has also been done, being that a Langmuir-Hinshelwood single site mechanism with dissociative adsorption of glycerol and molecular adsorption of water was proposed to describe the deposition of coke over a $Co-Ni/Al_2O_3$ catalyst. Despite this, more focus on this subject is required as well, so that the possible existence of different mechanisms of coke deposition on other types of catalysts may be disclosed.

Even if a good catalyst together with favoring operating conditions are used in catalytic GSR in a TR (e.g. fixed bed reactor), thermodynamic limitations in terms of glycerol conversion and hydrogen yield are still present. In order to avoid such constraints, intensified processes combining GSR reaction and CO_2 or H_2 selective removal in the same physical device have been found as an excellent alternative. It has been observed that removing CO_2 or H_2 from the reaction medium shifts the thermodynamic equilibrium towards higher glycerol conversions and higher hydrogen yields. Moreover, such processes allow to work at lower temperatures and attain similar or even better performances than TRs at higher temperatures. However, in order for the implementation of these processes be successful, CO_2 sorbents with high sorption capacity, stability and low sorption and regeneration temperatures (e.g. 300-500 °C), as well as hydrogen perm-selective membranes with high hydrogen selectivity and permeability and high resistance to embrittlement and poisoning have to be used. At the moment, hydrotalcite-based CO_2 sorbents (that require lower sorption and regeneration temperatures) and Pd-based membranes are seen as promising systems for use in SEGSR and GSR in MRs, respectively, at lower temperatures (300-400 °C). Moreover, appropriate operating conditions (temperature, WGFR, pressure and WHVS) have to be carefully chosen.

Regarding CO_2 emissions, these can be easily avoided though SEGSR, however MRs with H_2 perm-selective membranes are not efficient on this. On the other hand, highly pure H_2 streams suitable for use in PEMFCs can only be produced in MRs. Therefore, new solutions combining catalytic GSR with in situ CO_2 and H_2 removal would be interesting to explore.

8 References

[1] Zhou C-H, Beltramini JN, Fan Y-X, Lu GQ. Chemoselective catalytic conversion of glycerol as a biorenewable source to valuable commodity chemicals. Chemical Society Reviews. 2008;37:527-49.

[2] Dou B, Song Y, Wang C, Chen H, Xu Y. Hydrogen production from catalytic steam reforming of biodiesel byproduct glycerol: Issues and challenges. Renewable and Sustainable Energy Reviews. 2014;30:950-60.

[3] U.S. Energy Information Administration.

[4] Avasthi KS, Reddy RN, Patel S. Challenges in the Production of Hydrogen from Glycerol – A Biodiesel Byproduct Via Steam Reforming Process. Procedia Engineering. 2013;51:423-9.

[5] Ewan BCR, Allen RWK. A figure of merit assessment of the routes to hydrogen. International Journal of Hydrogen Energy. 2005;30:809-19.

[6] Liu Y, Farrauto R, Lawal A. Autothermal reforming of glycerol in a dual layer monolith catalyst. Chemical Engineering Science. 2013;89:31-9.

[7] Liu Y, Lawal A. Synthesis gas production by autothermal reforming of crude glycerol using a dual layer monolith catalyst. 2013.

[8] Nahar G, Dupont V. Recent advances in hydrogen production via autothermal reforming process (ATR): A review of patents and research articles. Recent Patents on Chemical Engineering. 2013;6:8-42.

[9] Wang W. Thermodynamic analysis of glycerol partial oxidation for hydrogen production. Fuel Processing Technology. 2010;91:1401-8.

[10] Camargo G, Cardozo S, Pena MV. Thermodynamical analysis of glycerol partial oxidation reaction using zeolites catalyst. 2012 AIChE Annual Meeting, AIChE 2012, October 28, 2012 - November 2, 2012. Pittsburgh, PA, United states: American Institute of Chemical Engineers; 2012.

[11] Liu S-K, Lin Y-C. Autothermal partial oxidation of glycerol to syngas over Pt-, LaMnO 3-, and Pt/LaMnO3-coated monoliths. Industrial and Engineering Chemistry Research. 2012;51:16278-87.

[12] Tuza PV, Manfro RL, Ribeiro NFP, Souza MMVM. Production of renewable hydrogen by aqueous-phase reforming of glycerol over Ni–Cu catalysts derived from hydrotalcite precursors. Renewable Energy. 2013;50:408-14.

[13] Ciftci A, Peng B, Jentys A, Lercher JA, Hensen EJM. Support effects in the aqueous phase reforming of glycerol over supported platinum catalysts. Applied Catalysis A: General. 2012;431–432:113-9.

[14] Manfro RL, da Costa AF, Ribeiro NFP, Souza MMVM. Hydrogen production by aqueous-phase reforming of glycerol over nickel catalysts supported on CeO2. Fuel Processing Technology. 2011;92:330-5.

[15] Byrd AJ, Pant KK, Gupta RB. Hydrogen production from glycerol by reforming in supercritical water over Ru/Al2O3 catalyst. Fuel. 2008;87:2956-60.

[16] Pairojpiriyakul T, Croiset E, Kiatkittipong W, Kiatkittipong K, Arpornwichanop A, Assabumrungrat S. Hydrogen production from catalytic supercritical water reforming of glycerol with cobalt-based catalysts. International Journal of Hydrogen Energy. 2013;38:4368-79.

[17] Gutiérrez Ortiz FJ, Serrera A, Galera S, Ollero P. Experimental study of the supercritical water reforming of glycerol without the addition of a catalyst. Energy. 2013;56:193-206.

[18] Dave CD, Pant KK. Renewable hydrogen generation by steam reforming of glycerol over zirconia promoted ceria supported catalyst. Renewable Energy. 2011;36:3195-202.

[19] Dieuzeide ML, Iannibelli V, Jobbagy M, Amadeo N. Steam reforming of glycerol over Ni/Mg/γ-Al2O3 catalysts. Effect of calcination temperatures. International Journal of Hydrogen Energy. 2012;37:14926-30.

[20] Dieuzeide ML, Jobbagy M, Amadeo N. Glycerol steam reforming over Ni/γ-Al2O3 catalysts, modified with Mg(II). Effect of Mg (II) content. Catalysis Today. 2013;213:50-7.

[21] Araque M, Martínez T LM, Vargas JC, Centeno MA, Roger AC. Effect of the active metals on the selective H2 production in glycerol steam reforming. Applied Catalysis B: Environmental. 2012;125:556-66.

[22] Iriondo A, Barrio VL, Cambra JF, Arias PL, Güemez MB, Navarro RM, et al. Influence of La2O3 modified support and Ni and Pt active phases on glycerol steam reforming to produce hydrogen. Catalysis Communications. 2009;10:1275-8.

[23] Araque M, Martínez T LM, Vargas JC, Roger AC. Hydrogen production by glycerol steam reforming over CeZrCo fluorite type oxides. Catalysis Today. 2011;176:352-6.

[24] Wang C, Dou B, Chen H, Song Y, Xu Y, Du X, et al. Hydrogen production from steam reforming of glycerol by Ni–Mg–Al based catalysts in a fixed-bed reactor. Chemical Engineering Journal. 2013;220:133-42.

[25] Wang X, Li S, Wang H, Liu B, Ma X. Thermodynamic analysis of glycerin steam reforming. Energy and Fuels. 2008;22:4285-91.

[26] Chen H, Ding Y, Cong NT, Dou B, Dupont V, Ghadiri M, et al. A comparative study on hydrogen production from steam-glycerol reforming: thermodynamics and experimental. Renewable Energy. 2011;36:779-88.

[27] Adhikari S, Fernando S, Haryanto A. A comparative thermodynamic and experimental analysis on hydrogen production by steam reforming of glycerin. Energy and Fuels. 2007;21:2306-10.

[28] Adhikari S, Fernando S, Gwaltney SR, Filip To SD, Mark Bricka R, Steele PH, et al. A thermodynamic analysis of hydrogen production by steam reforming of glycerol. International Journal of Hydrogen Energy. 2007;32:2875-80.

[29] Hajjaji N, Chahbani A, Khila Z, Pons M-N. A comprehensive energy–exergy-based assessment and parametric study of a hydrogen production process using steam glycerol reforming. Energy. 2014;64:473-83.

[30] Dieuzeide ML, Amadeo N. Thermodynamic analysis of Glycerol steam reforming. Chemical Engineering and Technology. 2010;33:89-96.

[31] Rossi CCRS, Alonso CG, Antunes OAC, Guirardello R, Cardozo-Filho L. Thermodynamic analysis of steam reforming of ethanol and glycerine for hydrogen production. International Journal of Hydrogen Energy. 2009;34:323-32.

[32] Fishtik I, Alexander A, Datta R, Geana D. Thermodynamic analysis of hydrogen production by steam reforming of ethanol via response reactions. International Journal of Hydrogen Energy. 2000;25:31-45.

[33] Mas V, Kipreos R, Amadeo N, Laborde M. Thermodynamic analysis of ethanol/water system with the stoichiometric method. International Journal of Hydrogen Energy. 2006;31:21-8.

[34] Authayanun S, Arpornwichanop A, Paengjuntuek W, Assabumrungrat S. Thermodynamic study of hydrogen production from crude glycerol autothermal reforming for fuel cell applications. International Journal of Hydrogen Energy. 2010;35:6617-23.

[35] Gutiérrez Ortiz FJ, Ollero P, Serrera A. Thermodynamic analysis of the autothermal reforming of glycerol using supercritical water. International Journal of Hydrogen Energy. 2011;36:12186-99.

[36] Gutiérrez Ortiz FJ, Ollero P, Serrera A, Sanz A. Thermodynamic study of the supercritical water reforming of glycerol. International Journal of Hydrogen Energy. 2011;36:8994-9013.

[37] Wang H, Wang X, Li M, Li S, Wang S, Ma X. Thermodynamic analysis of hydrogen production from glycerol autothermal reforming. International Journal of Hydrogen Energy. 2009;34:5683-90.

[38] Cheng CK, Foo SY, Adesina AA. Thermodynamic analysis of glycerol-steam reforming in the presence of CO 2 or H 2 as carbon gasifying agent. International Journal of Hydrogen Energy. 2012;37:10101-10.

[39] Authayanun S, Arpornwichanop A, Patcharavorachot Y, Wiyaratn W, Assabumrungrat S. Hydrogen production from glycerol steam reforming for low- and high-temperature PEMFCs. International Journal of Hydrogen Energy. 2011;36:267-75.

[40] Olajire AA. Valorization of greenhouse carbon dioxide emissions into value-added products by catalytic processes. Journal of CO2 Utilization. 2013;3–4:74-92.

[41] Li Y, Wang W, Chen B, Cao Y. Thermodynamic analysis of hydrogen production via glycerol steam reforming with CO2 adsorption. International Journal of Hydrogen Energy. 2010;35:7768-77.

[42] Chen H, Zhang T, Dou B, Dupont V, Williams P, Ghadiri M, et al. Thermodynamic analyses of adsorption-enhanced steam reforming of glycerol for hydrogen production. International Journal of Hydrogen Energy. 2009;34:7208-22.

[43] Lima da Silva A, Müller IL. Hydrogen production by sorption enhanced steam reforming of oxygenated hydrocarbons (ethanol, glycerol, n-butanol and methanol): Thermodynamic modelling. International Journal of Hydrogen Energy. 2011;36:2057-75.

[44] He L, Parra JMS, Blekkan EA, Chen D. Towards efficient hydrogen production from glycerol by sorption enhanced steam reforming. Energy and Environmental Science. 2010;3:1046-56.

[45] Wang X, Wang N, Li M, Li S, Wang S, Ma X. Hydrogen production by glycerol steam reforming with in situ hydrogen separation: A thermodynamic investigation. International Journal of Hydrogen Energy. 2010;35:10252-6.

[46] Lin Y-C. Catalytic valorization of glycerol to hydrogen and syngas. International Journal of Hydrogen Energy. 2013;38:2678-700.

[47] Adhikari S, Fernando SD, Haryanto A. Hydrogen production from glycerin by steam reforming over nickel catalysts. Renewable Energy. 2008;33:1097-100.

[48] Adhikari S, Fernando SD, To SDF, Bricka RM, Steele PH, Haryanto A. Conversion of glycerol to hydrogen via a steam reforming process over nickel catalysts. Energy and Fuels. 2008;22:1220-6.

[49] Sánchez EA, D'Angelo MA, Comelli RA. Hydrogen production from glycerol on Ni/Al2O3 catalyst. International Journal of Hydrogen Energy. 2010;35:5902-7.

[50] Pant KK, Jain R, Jain S. Renewable hydrogen production by steam reforming of glycerol over Ni/CeO 2 catalyst prepared by precipitation deposition method. Korean Journal of Chemical Engineering. 2011;28:1859-66.

[51] Nichele V, Signoretto M, Menegazzo F, Gallo A, Dal Santo V, Cruciani G, et al. Glycerol steam reforming for hydrogen production: Design of Ni supported catalysts. Applied Catalysis B: Environmental. 2012;111–112:225-32.

[52] Patel S, Pant KK. Production of hydrogen with low carbon monoxide formation via catalytic steam reforming of methanol. Journal of Fuel Cell Science and Technology. 2006;3:369-74.

[53] Iriondo A, Barrio VL, Cambra JF, Arias PL, Guemez MB, Sanchez-Sanchez MC, et al. Glycerol steam reforming over Ni catalysts supported on ceria and ceria-promoted alumina. International Journal of Hydrogen Energy. 2010;35:11622-33.

[54] Cui Y, Galvita V, Rihko-Struckmann L, Lorenz H, Sundmacher K. Steam reforming of glycerol: The experimental activity of La1–xCexNiO3 catalyst in comparison to the thermodynamic reaction equilibrium. Applied Catalysis B: Environmental. 2009;90:29-37.

[55] Franchini CA, Aranzaez W, Duarte de Farias AM, Pecchi G, Fraga MA. Ce-substituted LaNiO3 mixed oxides as catalyst precursors for glycerol steam reforming. Applied Catalysis B: Environmental. 2014;147:193-202.

[56] Adhikari S, Fernando S, Haryanto A. Production of hydrogen by steam reforming of glycerin over alumina-supported metal catalysts. Catalysis Today. 2007;129:355-64.

[57] Matas Güell B, Babich I, Nichols KP, Gardeniers JGE, Lefferts L, Seshan K. Design of a stable steam reforming catalyst—A promising route to sustainable hydrogen from biomass oxygenates. Applied Catalysis B: Environmental. 2009;90:38-44.

[58] Hagh BF. Optimization of autothermal reactor for maximum hydrogen production. International Journal of Hydrogen Energy. 2003;28:1369-77.

[59] Slinn M, Kendall K, Mallon C, Andrews J. Steam reforming of biodiesel by-product to make renewable hydrogen. Bioresource Technology. 2008;99:5851-8.

[60] Kim SM, Woo SI. Sustainable production of syngas from biomass-derived glycerol by steam reforming over highly stable Ni/SiC. ChemSusChem. 2012;5:1513-22.

[61] Wen G, Xu Y, Ma H, Xu Z, Tian Z. Production of hydrogen by aqueous-phase reforming of glycerol. International Journal of Hydrogen Energy. 2008;33:6657-66.

[62] Sanchez EA, Comelli RA. Hydrogen by glycerol steam reforming on a nickel–alumina catalyst: Deactivation processes and regeneration. International Journal of Hydrogen Energy. 2012;37:14740-6.

[63] Ni M, Leung DYC, Leung MKH. A review on reforming bio-ethanol for hydrogen production. International Journal of Hydrogen Energy. 2007;32:3238-47.

[64] Seo JG, Youn MH, Park S, Chung JS, Song IK. Hydrogen production by steam reforming of liquefied natural gas (LNG) over Ni/Al2O3-ZrO2 xerogel catalysts: Effect of calcination temperature of Al2O3-ZrO2 xerogel supports. International Journal of Hydrogen Energy. 2009;34:3755-63.

[65] Iriondo A, Cambra JF, Güemez MB, Barrio VL, Requies J, Sánchez-Sánchez MC, et al. Effect of ZrO2 addition on Ni/Al2O3 catalyst to produce H2 from glycerol. International Journal of Hydrogen Energy. 2012;37:7084-93.

[66] Huang Z-Y, Xu C-H, Meng J, Zheng C-F, Xiao H-W, Chen J, et al. Glycerol steam reforming to syngas over Ni-based catalysts on commercial Linde-type 5A zeolite modified by metal oxides. Journal of Environmental Chemical Engineering. in press.

[67] Iriondo A, Barrio VL, Cambra JF, Arias PL, Güemez MB, Navarro RM, et al. Hydrogen production from glycerol over nickel catalysts supported on Al2O3 modified by Mg, Zr, Ce or La. Topics in Catalysis. 2008;49:46-58.

[68] Buffoni IN, Pompeo F, Santori GF, Nichio NN. Nickel catalysts applied in steam reforming of glycerol for hydrogen production. Catalysis Communications. 2009;10:1656-60.

[69] Kitamura S, Su-Enaga T, Ikenaga NO, Miyake T, Suzuki T. Steam reforming of glycerin using Ni-based catalysts loaded on CaO-ZrO 2 solid solution. Catalysis Letters. 2011;141:895-905.

[70] Damyanova S, Bueno JMC. Effect of CeO2 loading on the surface and catalytic behaviors of CeO2-Al2O3-supported Pt catalysts. Applied Catalysis A: General. 2003;253:135-50.

[71] Takanabe K, Aika K-i, Seshan K, Lefferts L. Sustainable hydrogen from bio-oil—Steam reforming of acetic acid as a model oxygenate. Journal of Catalysis. 2004;227:101-8.

[72] Seo JG, Youn MH, Song IK. Hydrogen production by steam reforming of LNG over Ni/Al2O3–ZrO2 catalysts: Effect of Al2O3–ZrO2 supports prepared by a grafting method. Journal of Molecular Catalysis A: Chemical. 2007;268:9-14.

[73] Seo JG, Youn MH, Jung JC, Cho KM, Park S, Song IK. Preparation of Ni/Al2O3–ZrO2 catalysts and their application to hydrogen production by steam reforming of LNG: Effect of ZrO2 content grafted on Al2O3. Catalysis Today. 2008;138:130-4.

[74] Mawdsley JR, Krause TR. Rare earth-first-row transition metal perovskites as catalysts for the autothermal reforming of hydrocarbon fuels to generate hydrogen. Applied Catalysis A: General. 2008;334:311-20.

[75] Liguras DK, Kondarides DI, Verykios XE. Production of hydrogen for fuel cells by steam reforming of ethanol over supported noble metal catalysts. Applied Catalysis B: Environmental. 2003;43:345-54.

[76] Thyssen VV, Maia TA, Assaf EM. Ni supported on La2O3–SiO2 used to catalyze glycerol steam reforming. Fuel. 2013;105:358-63.

[77] Rostrup-Nielsen JR, Sehested J, Nørskov JK. Hydrogen and synthesis gas by steam- and C02 reforming. 2002. p. 65-139.

[78] Basagiannis AC, Verykios XE. Steam reforming of the aqueous fraction of bio-oil over structured Ru/MgO/Al2O3 catalysts. Catalysis Today. 2007;127:256-64.

[79] Huang ZY, Xu CH, Liu CQ, Xiao HW, Chen J, Zhang YX, et al. Glycerol steam reforming over Ni/γ-Al2O3 catalysts modified by metal oxides. Korean Journal of Chemical Engineering. 2013;30:587-92.

[80] Suelves I, Lázaro MJ, Moliner R, Echegoyen Y, Palacios JM. Characterization of NiAl and NiCuAl catalysts prepared by different methods for hydrogen production by thermo catalytic decomposition of methane. Catalysis Today. 2006;116:271-80.

[81] Maluf SS, Assaf EM. Ni catalysts with Mo promoter for methane steam reforming. Fuel. 2009;88:1547-53.

[82] Youn MH, Seo JG, Kim P, Song IK. Role and effect of molybdenum on the performance of Ni-Mo/γ-Al2O3 catalysts in the hydrogen production by auto-thermal reforming of ethanol. Journal of Molecular Catalysis A: Chemical. 2007;261:276-81.

[83] Huang T, Huang W, Huang J, Ji P. Methane reforming reaction with carbon dioxide over SBA-15 supported Ni-Mo bimetallic catalysts. Fuel Processing Technology. 2011;92:1868-75.

[84] Wu G, Li S, Zhang C, Wang T, Gong J. Glycerol steam reforming over perovskite-derived nickel-based catalysts. Applied Catalysis B: Environmental. 2014;144:277-85.

[85] Hakim L, Yaakob Z, Ismail M, Daud WRW, Sari R. Hydrogen production by steam reforming of glycerol over Ni/Ce/Cu hydroxyapatite-supported catalysts. Chemical Papers. 2013;67:703-12.

[86] Profeti LPR, Ticianelli EA, Assaf EM. Production of hydrogen via steam reforming of biofuels on Ni/CeO2–Al2O3 catalysts promoted by noble metals. International Journal of Hydrogen Energy. 2009;34:5049-60.

[87] Zhou CH, Zhao H, Tong DS, Wu LM, Yu WH. Recent advances in catalytic conversion of glycerol. Catalysis Reviews - Science and Engineering. 2013;55:369-453.

[88] Simonetti DA, Soares RR, Dumesic JA. Glycerol as a source for fuels and chemicals by low-temperature catalytic processing. 2006.

[89] Sutar PN, Vaidya PD, Rodrigues AE. Glycerol-reforming kinetics using a Pt/C catalyst. Chemical Engineering and Technology. 2010;33:1645-9.

[90] Simonetti DA, Kunkes EL, Dumesic JA. Gas-phase conversion of glycerol to synthesis gas over carbon-supported platinum and platinum-rhenium catalysts. Journal of Catalysis. 2007;247:298-306.

[91] Pompeo F, Santori GF, Nichio NN. Hydrogen production by glycerol steam reforming with Pt/SiO2 and Ni/SiO2 catalysts. Catalysis Today. 2011;172:183-8.

[92] Montini T, Singh R, Das P, Lorenzut B, Bertero N, Riello P, et al. Renewable H2 from glycerol steam reforming: Effect of La2O3 and CeO2 addition to Pt/Al2O3 catalysts. ChemSusChem. 2010;3:619-28.

[93] Kunkes EL, Soares RR, Simonetti DA, Dumesic JA. An integrated catalytic approach for the production of hydrogen by glycerol reforming coupled with water-gas shift. Applied Catalysis B: Environmental. 2009;90:693-8.

[94] Roh H-S, Potdar HS, Jeong D-W, Kim K-S, Shim J-O, Jang W-J, et al. Synthesis of highly active nano-sized (1 wt.% Pt/CeO2) catalyst for water gas shift reaction in medium temperature application. Catalysis Today. 2012;185:113-8.

[95] González ID, Navarro RM, Wen W, Marinkovic N, Rodriguéz JA, Rosa F, et al. A comparative study of the water gas shift reaction over platinum catalysts supported on CeO2, TiO2 and Ce-modified TiO2. Catalysis Today. 2010;149:372-9.

[96] Jeong D-W, Potdar HS, Shim J-O, Jang W-J, Roh H-S. H2 production from a single stage water–gas shift reaction over Pt/CeO2, Pt/ZrO2, and Pt/Ce(1−x)Zr(x)O2 catalysts. International Journal of Hydrogen Energy. 2013;38:4502-7.

[97] Pompeo F, Santori G, Nichio NN. Hydrogen and/or syngas from steam reforming of glycerol. Study of platinum catalysts. International Journal of Hydrogen Energy. 2010;35:8912-20.

[98] Gervasini A, Fenyvesi J, Auroux A. Study of the acidic character of modified metal oxide surfaces using the test of isopropanol decomposition. Catalysis Letters. 1997;43:219-28.

[99] Zhang XH, Yan FW, Guo CY, Yuan GQ. Steam reforming of glycerol over Pt-MCM-41 synthesized in a one-step process. Russian Journal of Physical Chemistry A. 2012;86:1957-61.

[100] Greeley J, Mavrikakis M. Alloy catalysts designed from first principles. Nature Materials. 2004;3:810-5.

[101] Ishikawa Y, Liao M-S, Cabrera CR. Energetics of H2O dissociation and COads+OHads reaction on a series of Pt–M mixed metal clusters: a relativistic density-functional study. Surface Science. 2002;513:98-110.

[102] Lehnert K, Claus P. Influence of Pt particle size and support type on the aqueous-phase reforming of glycerol. Catalysis Communications. 2008;9:2543-6.

[103] Frusteri F, Freni S, Spadaro L, Chiodo V, Bonura G, Donato S, et al. H2 production for MC fuel cell by steam reforming of ethanol over MgO supported Pd, Rh, Ni and Co catalysts. Catalysis Communications. 2004;5:611-5.

[104] Llorca J, Homs Ns, Sales J, Fierro J-LG, Ramírez de la Piscina P. Effect of sodium addition on the performance of Co–ZnO-based catalysts for hydrogen production from bioethanol. Journal of Catalysis. 2004;222:470-80.

[105] Batista MS, Santos RKS, Assaf EM, Assaf JM, Ticianelli EA. High efficiency steam reforming of ethanol by cobalt-based catalysts. Journal of Power Sources. 2004;134:27-32.

[106] Zhang B, Tang X, Li Y, Xu Y, Shen W. Hydrogen production from steam reforming of ethanol and glycerol over ceria-supported metal catalysts. International Journal of Hydrogen Energy. 2007;32:2367-73.

[107] Cheng CK, Foo SY, Adesina AA. H2-rich synthesis gas production over Co/Al2O3 catalyst via glycerol steam reforming. Catalysis Communications. 2010;12:292-8.

[108] Cheng CK, Foo SY, Adesina AA. Glycerol Steam Reforming over Bimetallic Co–Ni/Al2O3. Industrial & Engineering Chemistry Research. 2010;49:10804-17.

[109] Martínez T LM, Araque M, Vargas JC, Roger AC. Effect of Ce/Zr ratio in CeZr-CoRh catalysts on the hydrogen production by glycerol steam reforming. Applied Catalysis B: Environmental. 2013;132–133:499-510.

[110] Opoku-Gyamfi K, Adesina AA. Forced composition cycling of a novel thermally self-sustaining fluidised-bed reactor for methane reforming. Chemical Engineering Science. 1999;54:2575-83.

[111] Ambroise E, Courson C, Roger AC, Kiennemann A, Blanchard G, Rousseau S, et al. Exhaust gas recirculation for on-board hydrogen production by isooctane reforming: Comparison of performances of metal/ceria-zirconia based catalysts prepared through pseudo sol-gel or impregnation methods. Catalysis Today. 2010;154:133-41.

[112] Vargas JC, Libs S, Roger AC, Kiennemann A. Study of Ce-Zr-Co fluorite-type oxide as catalysts for hydrogen production by steam reforming of bioethanol. Catalysis Today. 2005;107-108:417-25.

[113] Romero-Sarria F, Vargas JC, Roger AC, Kiennemann A. Hydrogen production by steam reforming of ethanol. Study of mixed oxide catalysts Ce2Zr1.5Me0.5O8: Comparison of Ni/Co and effect of Rh. Catalysis Today. 2008;133-135:149-53.

[114] Sundari R, Vaidya PD. Reaction Kinetics of Glycerol Steam Reforming Using a Ru/Al2O3 Catalyst. Energy & Fuels. 2012;26:4195-204.

[115] Piscina PRDL, Homs N. Use of biofuels to produce hydrogen (reformation processes). Chemical Society Reviews. 2008;37:2459-67.

[116] Soria MA, Mateos-Pedrero C, Rodríguez-Ramos I, Guerrero-Ruiz A. Catalytic steam reforming of methane under conditions of applicability with Pd membranes over supported Ru catalysts. Catalysis Today. 2011;171:126-31.

[117] Hirai T, Ikenaga NO, Miyake T, Suzuki T. Production of hydrogen by steam reforming of glycerin on ruthenium catalyst. Energy and Fuels. 2005;19:1761-2.

[118] Nakagawa K, Hideshima S, Akamatsu N, Matsui NO, Ikenaga NO, Suzuki T. CO2 Reforming of Methane over Ru-Loaded Lanthanoid Oxide Catalysts. 2002. p. 205-23.

[119] Kim J, Lee D. Glycerol steam reforming on supported Ru-based catalysts for hydrogen production for fuel cells. International Journal of Hydrogen Energy. 2013;38:11853-62.

[120] Gallo A, Pirovano C, Marelli M, Psaro R, Dal Santo V. Hydrogen Production by Glycerol Steam Reforming with Ru-based Catalysts: A Study on Sn Doping. Chemical Vapor Deposition. 2010;16:305-10.

[121] Gallo A, Pirovano C, Ferrini P, Marelli M, Psaro R, Santangelo S, et al. Influence of reaction parameters on the activity of ruthenium based catalysts for glycerol steam reforming. Applied Catalysis B: Environmental. 2012;121–122:40-9.

[122] Dou B, Dupont V, Rickett G, Blakeman N, Williams PT, Chen H, et al. Hydrogen production by sorption-enhanced steam reforming of glycerol. Bioresource Technology. 2009;100:3540-7.

[123] Rass-Hansen J, Christensen CH, Sehested J, Helveg S, Rostrup-Nielsen JR, Dahl S. Renewable hydrogen: Carbon formation on Ni and Ru catalysts during ethanol steam-reforming. Green Chemistry. 2007;9:1016-21.

[124] Basagiannis AC, Verykios XE. Influence of the carrier on steam reforming of acetic acid over Ru-based catalysts. Applied Catalysis B: Environmental. 2008;82:77-88.

[125] Basile F, Fornasari G, Rosetti V, Trifirò F, Vaccari A. Effect of the Mg/Al ratio of the hydrotalcite-type precursor on the dispersion and activity of Rh and Ru catalysts for the partial oxidation of methane. Catalysis Today. 2004;91-92:293-7.

[126] Park SY, Kim JH, Moon DJ, Park NC, Kim YC. Autothermal reforming of propane over Ni-based hydrotalcite catalysts. Journal of Nanoscience and Nanotechnology. 2010;10:3175-9.

[127] Lee HJ, Lim YS, Park NC, Kim YC. Catalytic autothermal reforming of propane over the noble metal-doped hydrotalcite-type catalysts. Chemical Engineering Journal. 2009;146:295-301.

[128] Chiodo V, Freni S, Galvagno A, Mondello N, Frusteri F. Catalytic features of Rh and Ni supported catalysts in the steam reforming of glycerol to produce hydrogen. Applied Catalysis A: General. 2010;381:1-7.

[129] Palmeri N, Chiodo V, Freni S, Frusteri F, Bart JCJ, Cavallaro S. Hydrogen from oxygenated solvents by steam reforming on Ni/Al2O3 catalyst. International Journal of Hydrogen Energy. 2008;33:6627-34.

[130] Cavallaro S, Chiodo V, Freni S, Mondello N, Frusteri F. Performance of Rh/Al2O3 catalyst in the steam reforming of ethanol: H2 production for MCFC. Applied Catalysis A: General. 2003;249:119-28.

[131] Frusteri F, Spadaro L, Arena F, Chuvilin A. TEM evidence for factors affecting the genesis of carbon species on bare and K-promoted Ni/MgO catalysts during the dry reforming of methane. Carbon. 2002;40:1063-70.

[132] Bartholomew CH. CARBON DEPOSITION IN STEAM REFORMING AND METHANATION. Catalysis reviews. 1982;24:67-112.

[133] Ebshish A, Yaakob Z, Taufiq-Yap YH, Bshish A, Shaibani A. Catalytic Steam Reforming of Glycerol Over Cerium and Palladium-Based Catalysts for Hydrogen Production. Journal of Fuel Cell Science and Technology. 2013;10:021003-.

[134] Cheng CK, Foo SY, Adesina AA. Steam reforming of glycerol over Ni/Al2O3 catalyst. Catalysis Today. 2011;178:25-33.

[135] Adhikari S, Fernando SD, Haryanto A. Kinetics and Reactor Modeling of Hydrogen Production from Glycerol via Steam Reforming Process over Ni/CeO2 Catalysts. Chemical Engineering & Technology. 2009;32:541-7.

[136] Cheng CK, Foo SY, Adesina AA. Carbon deposition on bimetallic Co–Ni/Al2O3 catalyst during steam reforming of glycerol. Catalysis Today. 2011;164:268-74.

[137] Sundaram KM, Froment GF. Kinetics of coke deposition in the thermal cracking of propane. Chemical Engineering Science. 1979;34:635-44.

[138] Van Damme PS, Narayanan S, Froment GF. THERMAL CRACKING OF PROPANE AND PROPANE-PROPYLENE MIXTURES: PILOT PLANT VERSUS INDUSTRIAL DATA. AIChE Journal. 1975;21:1065-73.

[139] Dou B, Wang C, Chen H, Song Y, Xie B. Continuous sorption-enhanced steam reforming of glycerol to high-purity hydrogen production. International Journal of Hydrogen Energy. 2013;38:11902-9.

[140] Hanif A, Dasgupta S, Divekar S, Arya A, Garg MO, Nanoti A. A study on high temperature CO2 capture by improved hydrotalcite sorbents. Chemical Engineering Journal. 2014;236:91-9.

[141] Maroño M, Torreiro Y, Gutierrez L. Influence of steam partial pressures in the CO2 capture capacity of K-doped hydrotalcite-based sorbents for their application to SEWGS processes. International Journal of Greenhouse Gas Control. 2013;14:183-92.

[142] Martunus, Helwani Z, Wiheeb AD, Kim J, Othman MR. Improved carbon dioxide capture using metal reinforced hydrotalcite under wet conditions. International Journal of Greenhouse Gas Control. 2012;7:127-36.

[143] Aschenbrenner O, McGuire P, Alsamaq S, Wang J, Supasitmongkol S, Al-Duri B, et al. Adsorption of carbon dioxide on hydrotalcite-like compounds of different compositions. Chemical Engineering Research and Design. 2011;89:1711-21.

[144] Wang Q, Tay HH, Guo Z, Chen L, Liu Y, Chang J, et al. Morphology and composition controllable synthesis of Mg–Al–CO3 hydrotalcites by tuning the synthesis pH and the CO2 capture capacity. Applied Clay Science. 2012;55:18-26.

[145] Wang Y, Zhu Y, Wu S. A new nano CaO-based CO2 adsorbent prepared using an adsorption phase technique. Chemical Engineering Journal. 2013;218:39-45.

[146] Sanchez-Jimenez PE, Perez-Maqueda LA, Valverde JM. Nanosilica supported CaO: A regenerable and mechanically hard CO2 sorbent at Ca-looping conditions. Applied Energy. 2014;118:92-9.

[147] Zhang X, Li Z, Peng Y, Su W, Sun X, Li J. Investigation on a novel CaO-Y2O3 sorbent for efficient CO2 mitigation. Chemical Engineering Journal. 2014;243:297-304.

[148] Nieto-Sanchez AJ, Olivares-Marin M, Garcia S, Pevida C, Cuerda-Correa EM. Influence of the operation conditions on CO2 capture by CaO-derived sorbents prepared from synthetic CaCO3. Chemosphere. 2013;93:2148-58.

[149] Akgsornpeak A, Witoon T, Mungcharoen T, Limtrakul J. Development of synthetic CaO sorbents via CTAB-assisted sol–gel method for CO2 capture at high temperature. Chemical Engineering Journal. 2014;237:189-98.

[150] Wang S, An C, Zhang Q-H. Syntheses and structures of lithium zirconates for high-temperature CO2 absorption. Journal of Materials Chemistry A. 2013;1:3540-50.

[151] Duan Y. Structural and electronic properties of Li8ZrO6 and its CO2 capture capabilities: an ab initio thermodynamic approach. Physical Chemistry Chemical Physics. 2013;15:9752-60.

[152] Xiao Q, Tang X, Liu Y, Zhong Y, Zhu W. Citrate route to prepare K-doped Li2ZrO3 sorbents with excellent CO2 capture properties. Chemical Engineering Journal. 2011;174:231-5.

[153] Halabi MH, de Croon MHJM, van der Schaaf J, Cobden PD, Schouten JC. Reactor modeling of sorption-enhanced autothermal reforming of methane. Part I: Performance study of hydrotalcite and lithium zirconate-based processes. Chemical Engineering Journal. 2011;168:872-82.

[154] Iwan A, Stephenson H, Ketchie WC, Lapkin AA. High temperature sequestration of CO2 using lithium zirconates. Chemical Engineering Journal. 2009;146:249-58.

[155] Mizunuma M, Tsuda M, Maruo Y, Nakagaki T. CO2 Capture System Using Lithium Silicate for Distributed Power Supply. Energy Procedia. 2013;37:1194-201.

[156] Seggiani M, Puccini M, Vitolo S. Alkali promoted lithium orthosilicate for CO2 capture at high temperature and low concentration. International Journal of Greenhouse Gas Control. 2013;17:25-31.

[157] Chowdhury MBI, Quddus MR, deLasa HI. CO2 capture with a novel solid fluidizable sorbent: Thermodynamics and Temperature Programmed Carbonation–Decarbonation. Chemical Engineering Journal. 2013;232:139-48.

[158] Shan S, Jia Q, Jiang L, Li Q, Wang Y, Peng J. Novel Li4SiO4-based sorbents from diatomite for high temperature CO2 capture. Ceramics International. 2013;39:5437-41.

[159] Duan Y, Pfeiffer H, Li B, Romero-Ibarra IC, Sorescu DC, Luebke DR, et al. CO2 capture properties of lithium silicates with different ratios of Li2O/SiO2: an ab initio thermodynamic and experimental approach. Physical Chemistry Chemical Physics. 2013;15:13538-58.

[160] Yong Z, Rodrigues ArE. Hydrotalcite-like compounds as adsorbents for carbon dioxide. Energy Conversion and Management. 2002;43:1865-76.

[161] Yong Z, Mata V, Rodrigues ArE. Adsorption of carbon dioxide at high temperature—a review. Separation and Purification Technology. 2002;26:195-205.

[162] Yong Z, Mata V, Rodrigues A. Adsorption of Carbon Dioxide on Chemically Modified High Surface Area Carbon-Based Adsorbents at High Temperature. Adsorption. 2001;7:41-50.

[163] Gupta H, Fan L-S. Carbonation–Calcination Cycle Using High Reactivity Calcium Oxide for Carbon Dioxide Separation from Flue Gas. Industrial & Engineering Chemistry Research. 2002;41:4035-42.

[164] L. G. Oliveira E. Sorption enhanced steam methane reforming process for continuous production of hydrogen in pressure swing adsorptive reactors: University of Porto; 2009.

[165] Carlos VM, Raquel T, Vicente R, Miguel AV, Alexandre FPF, Alírio ER, et al. High Temperature CO2 Sorption with Gallium-Substituted and Promoted Hydrotalcites. Separation and Purification Technology. in press.

[166] Lu H, Reddy EP, Smirniotis PG. Calcium oxide based sorbents for capture of carbon dioxide at high temperatures. Industrial and Engineering Chemistry Research. 2006;45:3944-9.

[167] Wang L, Li D, Watanabe H, Tamura M, Nakagawa Y, Tomishige K. Catalytic performance and characterization of Co/Mg/Al catalysts prepared from hydrotalcite-like precursors for the steam gasification of biomass. Applied Catalysis B: Environmental. 2014;150–151:82-92.

[168] Wang Q, Wu Z, Tay HH, Chen L, Liu Y, Chang J, et al. High temperature adsorption of CO2 on Mg–Al hydrotalcite: Effect of the charge compensating anions and the synthesis pH. Catalysis Today. 2011;164:198-203.

[169] Fermoso J, He L, Chen D. Production of high purity hydrogen by sorption enhanced steam reforming of crude glycerol. International Journal of Hydrogen Energy. 2012;37:14047-54.

[170] Dou B, Rickett GL, Dupont V, Williams PT, Chen H, Ding Y, et al. Steam reforming of crude glycerol with in situ CO2 sorption. Bioresource Technology. 2010;101:2436-42.

[171] Chen H, Ding Y, Cong NT, Dou B, Dupont V, Ghadiri M, et al. Progress in low temperature hydrogen production with simultaneous CO2 abatement. Chemical Engineering Research and Design. 2011;89:1774-82.

[172] Wang X, Li M, Li S, Wang H, Wang S, Ma X. Hydrogen production by glycerol steam reforming with/without calcium oxide sorbent: A comparative study of thermodynamic and experimental work. Fuel Processing Technology. 2010;91:1812-8.

[173] Terminology for membranes and membrane processes (IUPAC Recommendation 1996). Journal of Membrane Science. 1996;120:149-59.

[174] Haag S, Burgard M, Ernst B. Beneficial effects of the use of a nickel membrane reactor for the dry reforming of methane: Comparison with thermodynamic predictions. Journal of Catalysis. 2007;252:190-204.

[175] Gallucci F, Fernandez E, Corengia P, van Sint Annaland M. Recent advances on membranes and membrane reactors for hydrogen production. Chemical Engineering Science. 2013;92:40-66.

[176] Adhikari S, Fernando S. Hydrogen membrane separation techniques. Industrial and Engineering Chemistry Research. 2006;45:875-81.

[177] Miguel CV, Mendes A, Tosti S, Madeira LM. Effect of CO and CO2 on H2 permeation through finger-like Pd–Ag membranes. International Journal of Hydrogen Energy. 2012;37:12680-7.

[178] Tosti S, Basile A, Bettinali L, Borgognoni F, Chiaravalloti F, Gallucci F. Long-term tests of Pd–Ag thin wall permeator tube. Journal of Membrane Science. 2006;284:393-7.

[179] Mendes D, Mendes A, Madeira LM, Iulianelli A, Sousa JM, Basile A. The water-gas shift reaction: From conventional catalytic systems to Pd-based membrane reactors- A review. Asia-Pacific Journal of Chemical Engineering. 2010;5:111-37.

[180] Mendes D, Chibante V, Zheng JM, Tosti S, Borgognoni F, Mendes A, et al. Enhancing the production of hydrogen via water-gas shift reaction using Pd-based membrane reactors. International Journal of Hydrogen Energy. 2010;35:12596-608.

[181] Santucci A, Borgognoni F, Vadrucci M, Tosti S. Testing of dense Pd–Ag tubes: Effect of pressure and membrane thickness on the hydrogen permeability. Journal of Membrane Science. 2013;444:378-83.

[182] Nayebossadri S, Speight J, Book D. Effects of low Ag additions on the hydrogen permeability of Pd–Cu–Ag hydrogen separation membranes. Journal of Membrane Science. 2014;451:216-25.

[183] Lewis AE, Kershner DC, Paglieri SN, Slepicka MJ, Way JD. Pd–Pt/YSZ composite membranes for hydrogen separation from synthetic water–gas shift streams. Journal of Membrane Science. 2013;437:257-64.

[184] Wei L, Yu J, Huang Y. Silver coating on porous stainless steel substrate and preparation of H2-permeable palladium membranes. International Journal of Hydrogen Energy. 2013;38:10833-8.

[185] Wei L, Yu J, Hu X, Huang Y. Fabrication of H2-permeable palladium membranes based on pencil-coated porous stainless steel substrate. International Journal of Hydrogen Energy. 2012;37:13007-12.

[186] Zhang D, Zhou S, Fan Y, Xu N, He Y. Preparation of dense Pd composite membranes on porous Ti–Al alloy supports by electroless plating. Journal of Membrane Science. 2012;387–388:24-9.

[187] Braun F, Tarditi AM, Miller JB, Cornaglia LM. Pd-based binary and ternary alloy membranes: Morphological and perm-selective characterization in the presence of H2S. Journal of Membrane Science. 2014;450:299-307.

[188] Basile A, Gallucci F, Iulianelli A, Tereschenko GF, Ermilova MM, Orekhova NV. Ti–Ni–Pd dense membranes—The effect of the gas mixtures on the hydrogen permeation. Journal of Membrane Science. 2008;310:44-50.

[189] Peters TA, Kaleta T, Stange M, Bredesen R. Development of thin binary and ternary Pd-based alloy membranes for use in hydrogen production. Journal of Membrane Science. 2011;383:124-34.

[190] Chang ACC, Lin W-H, Lin K-H, Hsiao C-H, Chen H-H, Chang H-F. Reforming of glycerol for producing hydrogen in a Pd/Ag membrane reactor. International Journal of Hydrogen Energy. 2012;37:13110-7.

[191] Iulianelli A, Longo T, Liguori S, Basile A. Production of hydrogen via glycerol steam reforming in a Pd-Ag membrane reactor over Co-Al2O3 catalyst. Asia-Pacific Journal of Chemical Engineering. 2010;5:138-45.

[192] Lin K-H, Lin W-H, Hsiao C-H, Chang H-F, Chang ACC. Hydrogen production in steam reforming of glycerol by conventional and membrane reactors. International Journal of Hydrogen Energy. 2012;37:13770-6.

[193] Iulianelli A, Seelam PK, Liguori S, Longo T, Keiski R, Calabrò V, et al. Hydrogen production for PEM fuel cell by gas phase reforming of glycerol as byproduct of bio-diesel. The use of a Pd–Ag membrane reactor at middle reaction temperature. International Journal of Hydrogen Energy. 2011;36:3827-34.
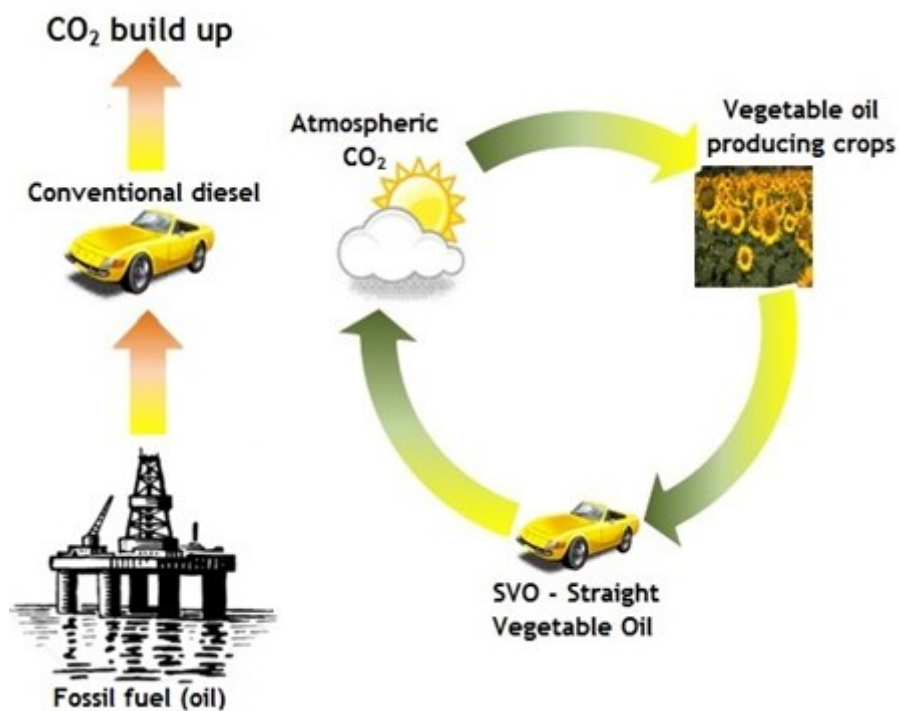
Figures Captions

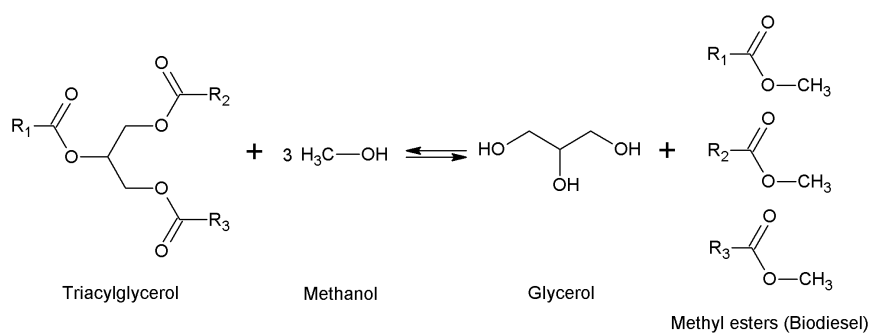**Fig. 1 -** Comparison of CO_2 emission cycles between conventional diesel and biodiesel.

Fig. 2 – Overall reaction of triglycerides transesterification with methanol for biodiesel production yielding glycerol as by-product.
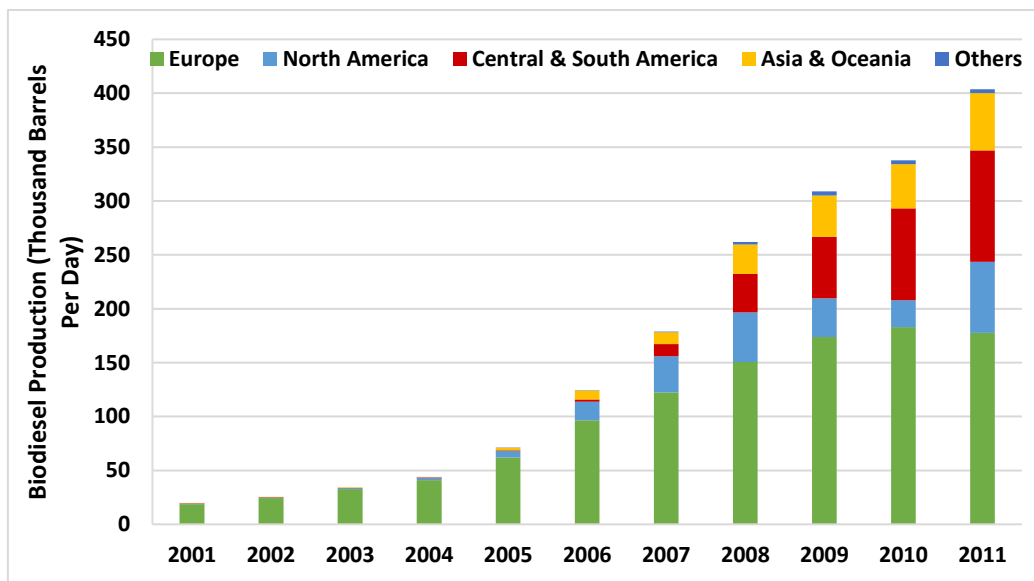
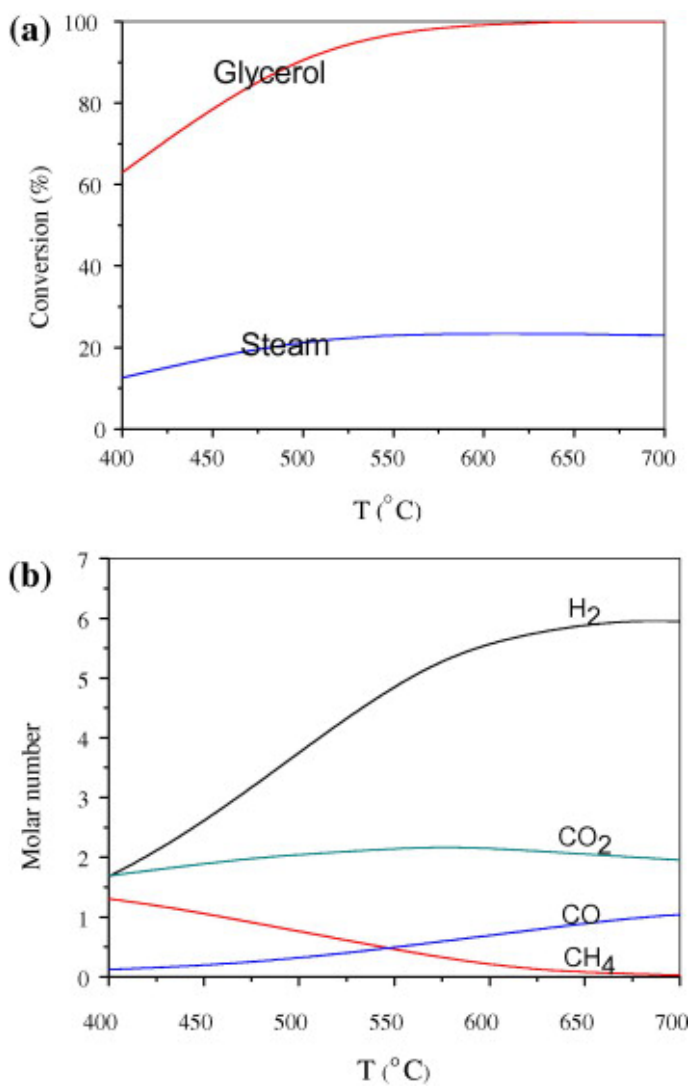**Fig. 3 -** Evolution of worldwide biodiesel production between 2001-2011 [3].

Fig. 4 - Thermodynamic equilibrium of GSR: (a) Glycerol and steam conversions and (b) moles of gas products. Water/glycerol feed ratio (WGFR) = 9, atmospheric pressure and considering eq. (2, 5 and 6). Reprinted from Chemical Engineering Journal, 220, Wang C, Dou B, Chen H,
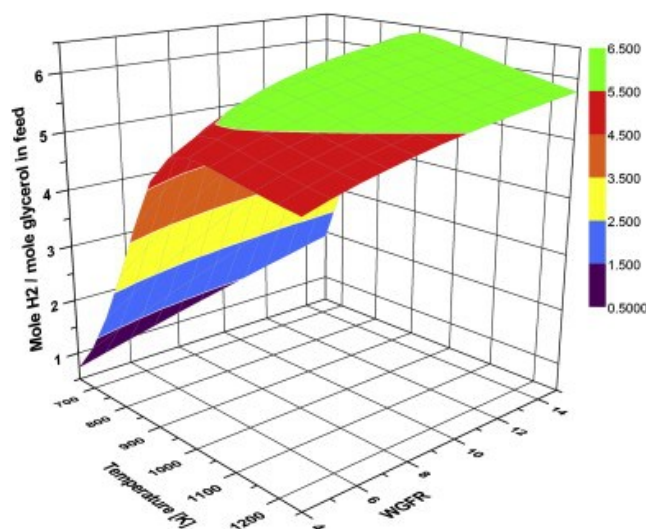
Fig. 5 - Moles of H_2 produced per mole of glycerol during GSR as function of WGFR and temperature at 1 atm and considering eq. (2, 3, 5 and 6). Reprinted from Energy, 64, Hajjaji N, Chahbani A, Khila Z, Pons M-N., A comprehensive energy–exergy-based assessment and parametric study of a hydrogen production process using steam glycerol reforming, 473-83, Copyright (2014), with permission from Elsevier.
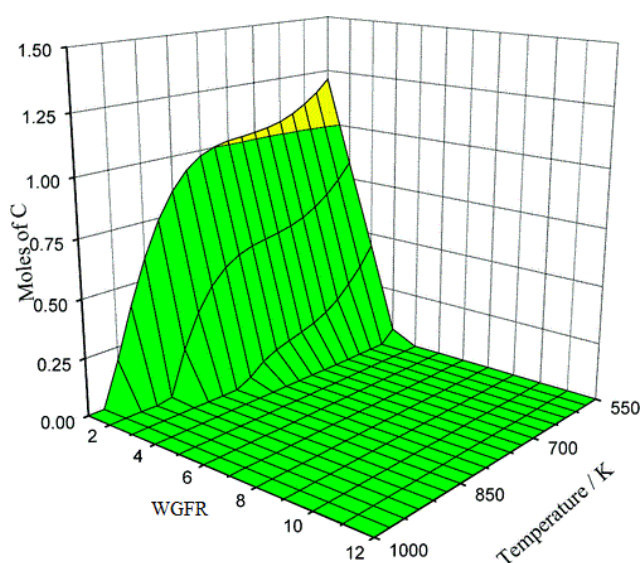
Fig. 6 - Moles of carbon formed as a function of WGFR and temperature at 50 atm. Adapted with permission from (Wang X, Li S, Wang H, Liu B, Ma X. Thermodynamic analysis of glycerin steam reforming. Energy and Fuels. 2008; 22:4285-91). Copyright (2008) American Chemical Society.
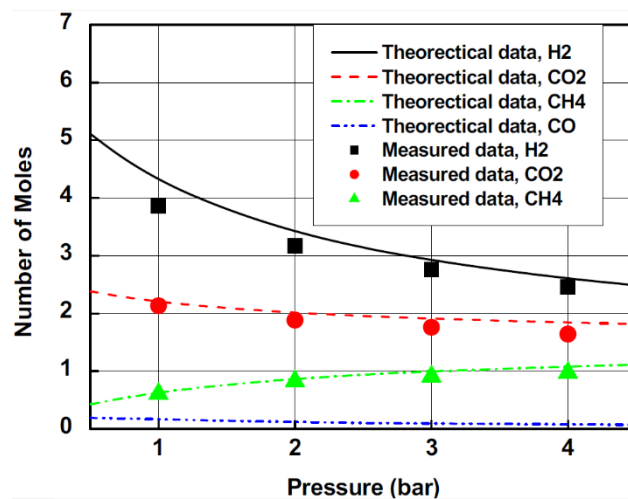
Fig. 7 - Effect of total pressure on the number of moles of different components in the equilibrium. T = 450 °C, WGFR = 9, feeding reactants to inert gas ratio = 1:4. Reprinted from Renewable Energy, 36, Chen H, Ding Y, Cong NT, Dou B, Dupont V, Ghadiri M, et al., A comparative study on hydrogen production from steam-glycerol reforming: thermodynamics and experimental, 779-88, Copyright (2011), with permission from Elsevier.
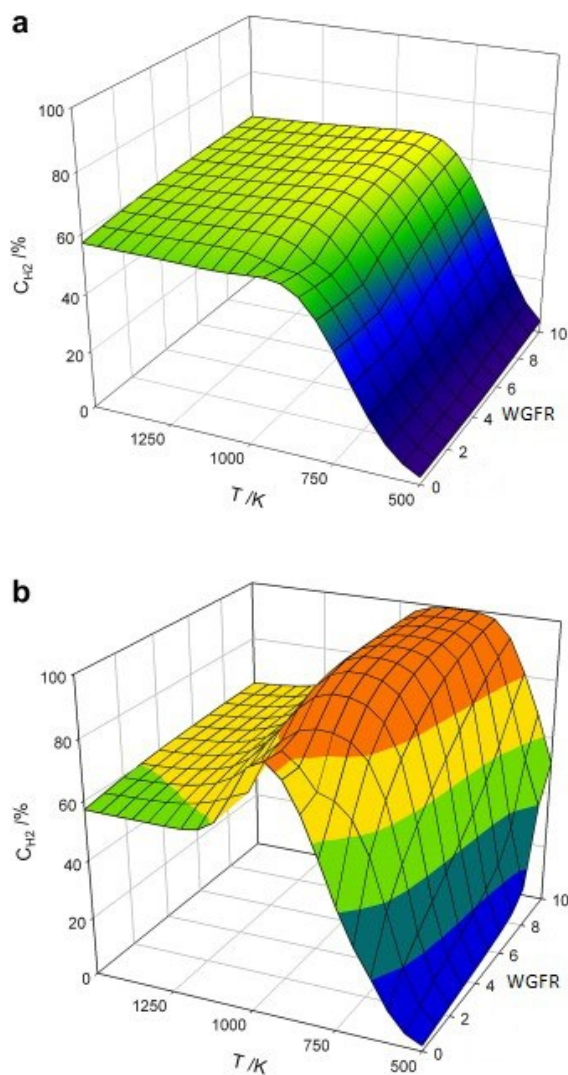
Fig. 8 - Hydrogen concentration (dry basis) in equilibrium as function of temperature and WGFR in (a) GSR and (b) SEGSR, at 1 atm. Adapted from International Journal of Hydrogen Energy, 35, Li Y, Wang W, Chen B, Cao Y, Thermodynamic analysis of hydrogen production via glycerol steam reforming with CO2 adsorption, 7768-77, Copyright (2010), with permission from International Journal of Hydrogen Energy.
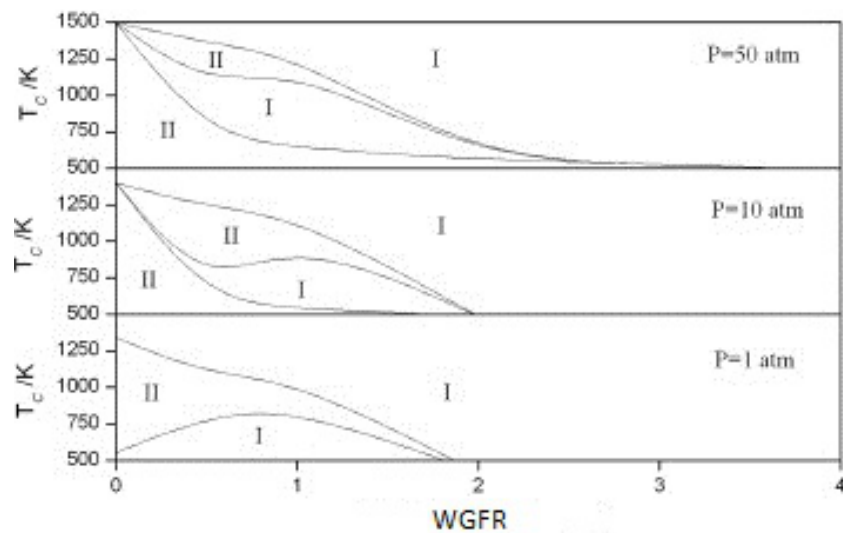

Fig. 9 - Coke free (I) and coke formed (II) regions in SEGSR as a function of temperature and WGFR, at 1 atm, 10 atm and 50 atm. Reprinted from International Journal of Hydrogen Energy, 35, Li Y, Wang W, Chen B, Cao Y, Thermodynamic analysis of hydrogen production via glycerol steam reforming with CO2 adsorption, 7768-77, Copyright (2010), with permission from International Journal of Hydrogen Energy.
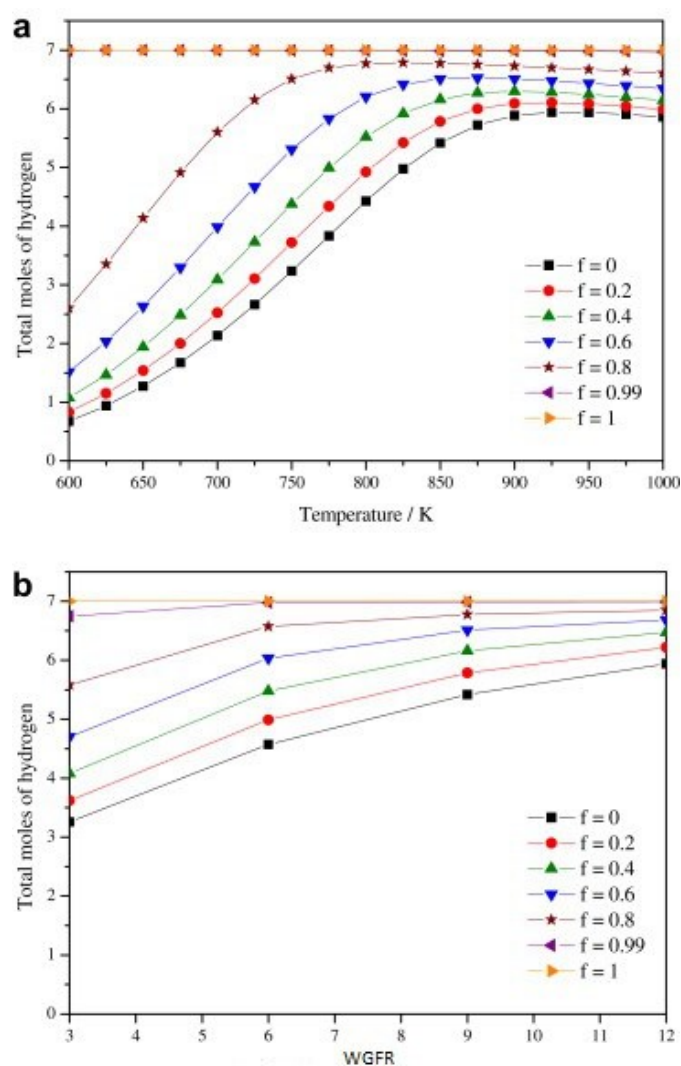
Fig. 10 - Effect of (a) temperature (WGFR = 9) and (b) WGFR (T = 850 K) at 1 atm and fraction of hydrogen removal (f) on the production of H_2. Adapted from International Journal of Hydrogen Energy, 35, Wang X, Wang N, Li M, Li S, Wang S, Ma X, Hydrogen production by glycerol steam reforming with in situ hydrogen separation: A thermodynamic investigation, 10252-6, Copyright (2010), with permission from International Journal of Hydrogen Energy.
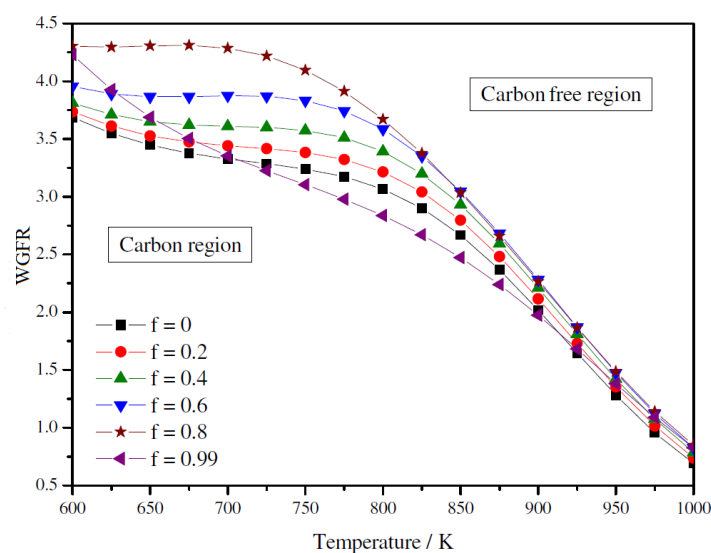
Fig. 11 - Carbon formation as function of WGFR and temperature at 1 atm, for different values of f. Adapted from International Journal of Hydrogen Energy, 35, Wang X, Wang N, Li M, Li S, Wang S, Ma X, Hydrogen production by glycerol steam reforming with in situ hydrogen separation: A thermodynamic investigation, 10252-6, Copyright (2010), with permission from International Journal of Hydrogen Energy.
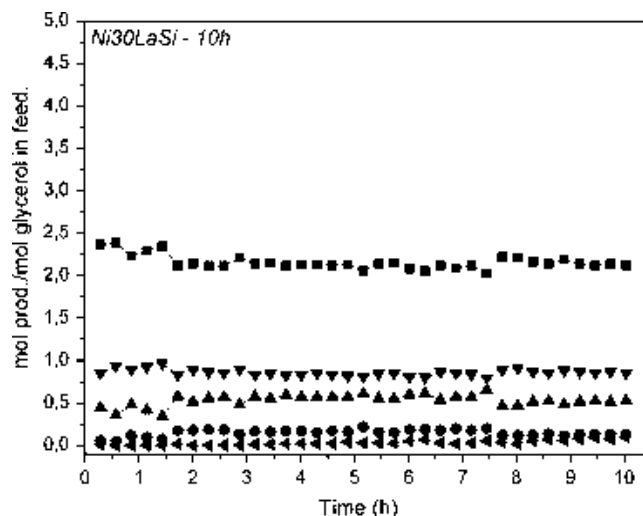

Fig. 12 - Yield of gaseous products formed during the stability reaction of GSR with the 30 wt.% La_2O_3 content catalyst (■H_2 ● CH_4 ▲ CO ▼ CO_2 ◀ C_2H_4). Reprinted from Fuel, 105, Thyssen VV, Maia TA, Assaf EM., Ni supported on La2O3–SiO2 used to catalyze glycerol steam reforming, 358-63, Copyright (2013), with permission from Elsevier.
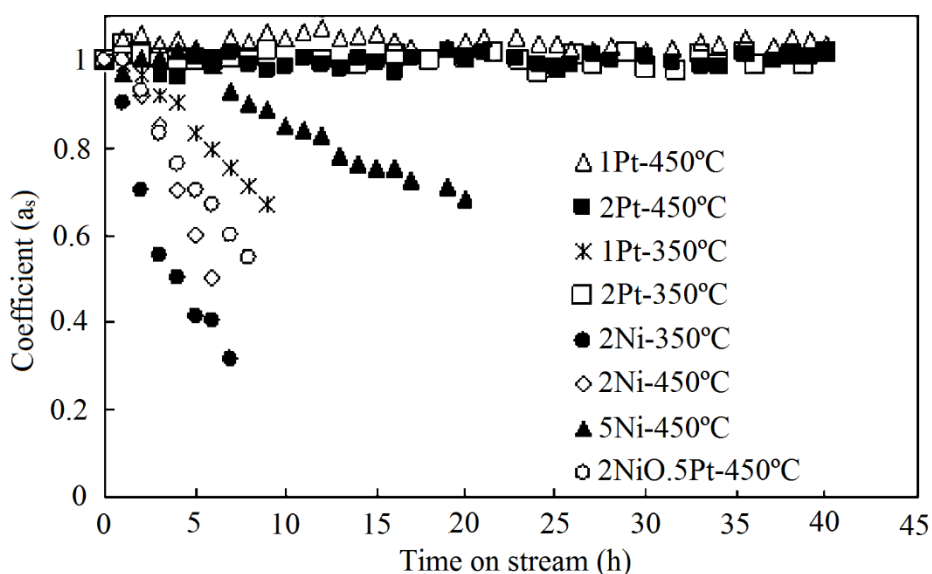

Fig. 13 - Activity over time-on-stream at 350 °C and 450 °C with different catalysts supported on SiO_2 (feed flow rate of 0.5 mL·min^{-1}, 10 wt.% aqueous solution of glycerol and for a residence time of 0.88 min). Reprinted from Catalysis Today, 172, Pompeo F, Santori GF, Nichio NN., Hydrogen production by glycerol steam reforming with Pt/SiO2 and Ni/SiO2 catalysts, 183-8, Copyright (2011), with permission from Elsevier.
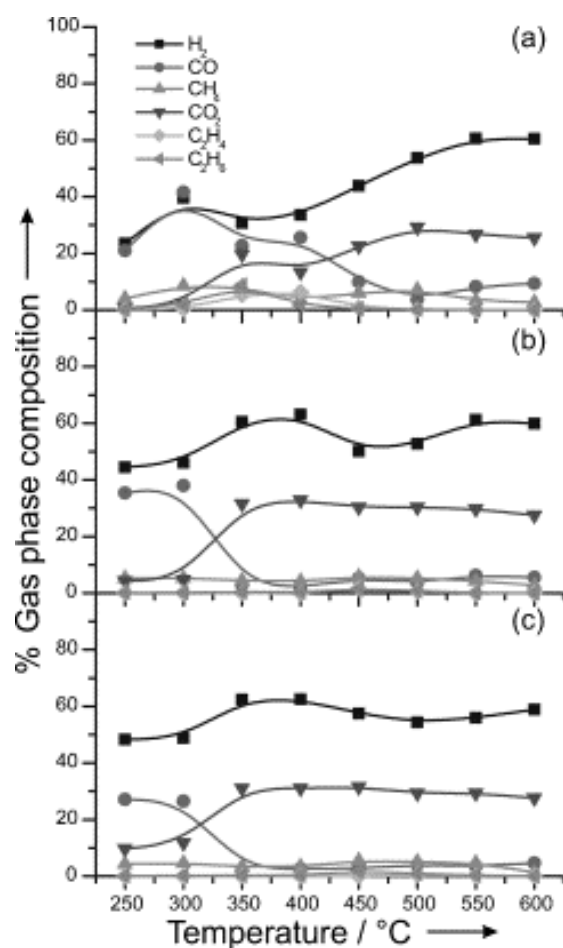
Fig. 14 - Stability tests over doped Pt/Al$_2$O$_3$ catalysts. Top: glycerol conversion to gas-phase products. Bottom: gas-phase composition using (a) Pt/La$_2$O$_3$/Al$_2$O$_3$ and (b) Pt/CeO$_2$/Al$_2$O$_3$ catalyst. Conditions: 1.00 g catalyst, 0.32 mL·min^{-1} of C$_3$H$_8$O$_3$ (30 wt.%; aqueous solution), T = 350 °C. Reprinted from ChemSusChem., 3, Montini T, Singh R, Das P, Lorenzut B, Bertero N, Riello P, et al., Renewable H2 from glycerol steam reforming: Effect of La2O3 and CeO2 addition to Pt/Al2O3 catalysts, 619-28, Copyright © 2010 WILEY-VCH Verlag GmbH & Co. KGaA, Weinheim.
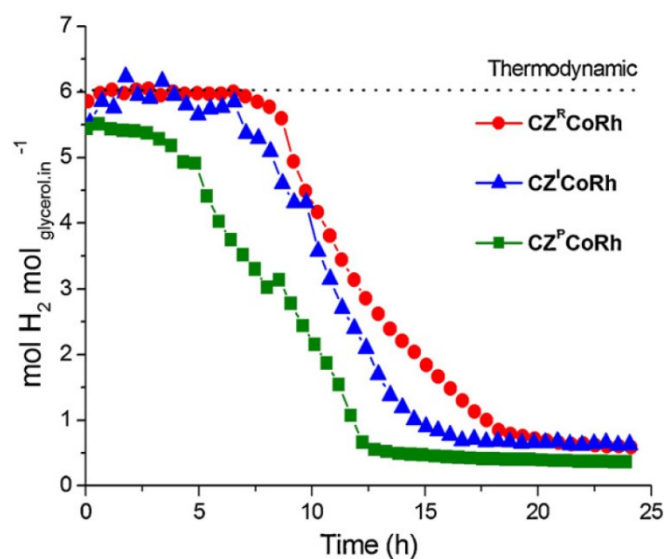
Fig. 15 - Evolution of the H_2 production in GSR over $Ce_{0.53}Zr_{2.97}Co_{0.47}Rh_{0.03}O_{8-\delta}$ with poor ceria content (CZ^{P}CoRh), $Ce_2Zr_{1.5}Co_{0.47}Rh_{0.03}O_{8-\delta}$ with intermediate ceria content (CZ^{I}CoRh), and $Ce_{2.59}Zr_{0.91}Co_{0.47}Rh_{0.03}O_{8-\delta}$ with rich ceria content (CZ^{R}CoRh). Conditions: temperature 650 ºC, WGFR of 9 and atmospheric pressure. Thermodynamic value expected using the UNIQUAC model: 6.06 $molH_2 \cdot mol_{glycerol.in}^{-1}$. Reprinted from Applied Catalysis B: Environmental, 132–133, Martínez T LM, Araque M, Vargas JC, Roger AC., Effect of Ce/Zr ratio in CeZr-CoRh catalysts on the hydrogen production by glycerol steam reforming, 499-510, Copyright (2013), with permission from Elsevier.
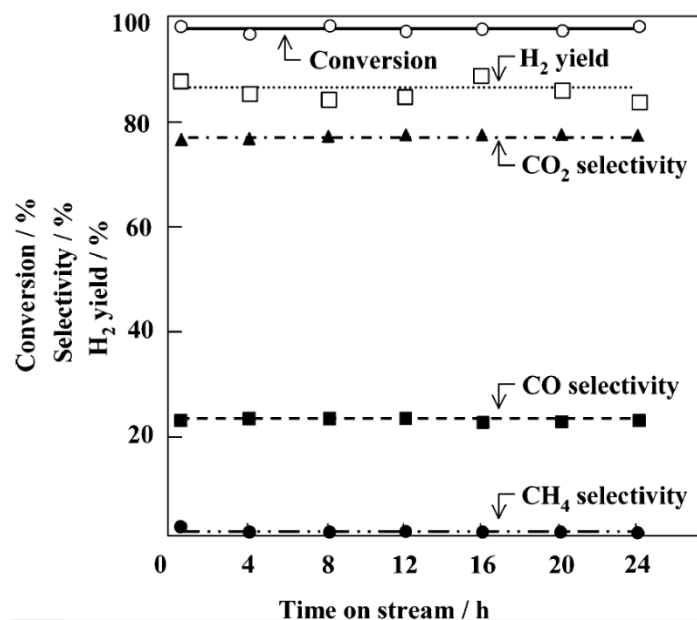

Fig. 16 - Stability tests over 3 wt.% Ru/Y_2O_3 catalyst for 24 h in the GSR, at 600 ºC and sweep gas space velocity of 80 000 $mL \cdot g_{cat}^{-1} \cdot h^{-1}$. Reprinted with permission from (Hirai T, Ikenaga NO, Miyake T, Suzuki T. Production of hydrogen by steam reforming of glycerin on ruthenium catalyst. Energy and Fuels. 2005;19:1761-2). Copyright (2005) American Chemical Society.
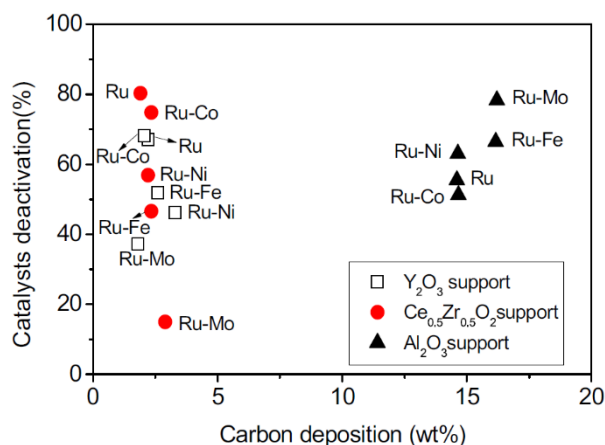
Fig. 17 - Deactivation of catalysts (%) with respect to the amount of solid carbonaceous species deposited (wt.%) on the catalysts after 10 h of reaction at 600 ºC (feed conditions: WGFR of 12, spatial velocity of 876-2340 $\mu mol \cdot g_{cat.}^{-1} \cdot min^{-1}$). Reprinted from International Journal of Hydrogen Energy, 38, Kim J, Lee D, Glycerol steam reforming on supported Ru-based catalysts for hydrogen production for fuel cells, 11853-62, Copyright (2013), with permission from International Journal of Hydrogen Energy.

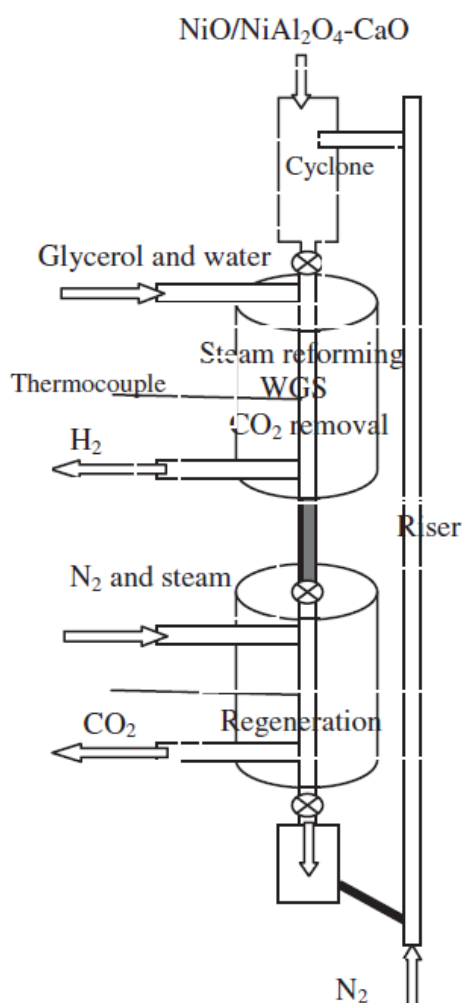**Fig. 18 -** Scheme of the continuous SEGSR system. Reprinted from International Journal of Hydrogen Energy, 38, Dou B, Wang C, Chen H, Song Y, Xie B, Continuous sorption-enhanced steam reforming of glycerol to high-purity hydrogen production, 11902-9, Copyright (2013), with permission from International Journal of Hydrogen Energy.
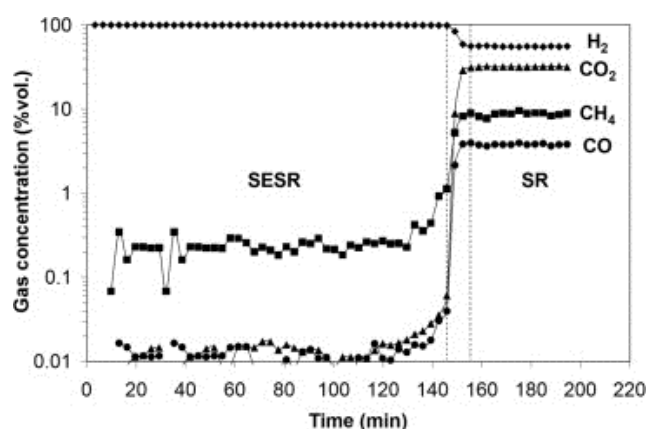
Fig. 19 - Evolution with time of the gas product composition (N_2 free and dry basis) during SEGSR at 550 °C, WGFR of 9, 1 atm, contact time of 1.09 h and sorbent/catalyst = 5). Reprinted from International Journal of Hydrogen Energy, 37, Fermoso J, He L, Chen D, Production of high purity hydrogen by sorption enhanced steam reforming of crude glycerol, 14047-54, Copyright (2012), with permission from International Journal of Hydrogen Energy.

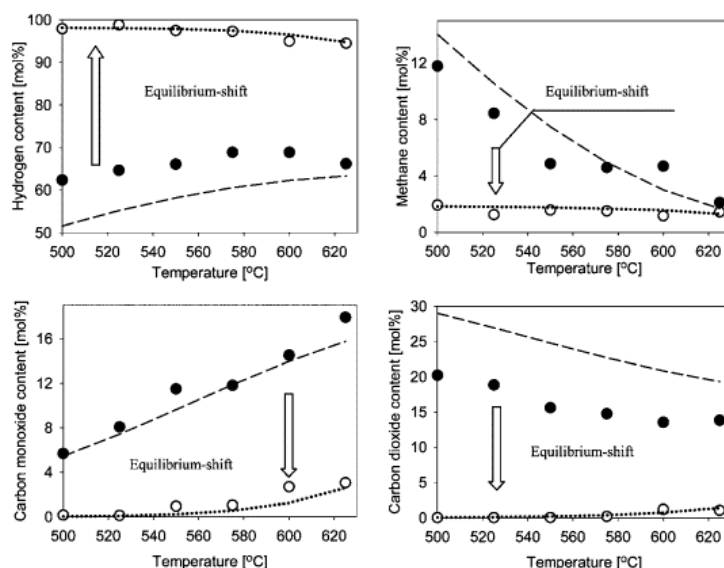**Fig. 20 -** Product gas composition (dry basis) of GSR with and without in situ CO_2 removal at WGFR of 4, 1 atm, catalyst/sorbent ratio of 5/2.5 and contact time of 1 h (··· thermodynamic equilibrium of SEGSR, --- thermodynamic equilibrium of GSR, O experimental results for SEGSR, ● experimental results for GSR). [He L, Parra JMS, Blekkan EA, Chen D. Towards efficient hydrogen production from glycerol by sorption enhanced steam reforming. Energy and Environmental Science. 2010;3:1046-56] - Reproduced by permission of The Royal Society of Chemistry. Available at http://pubs.rsc.org/en/content/articlepdf/2010/ee/b922355j.
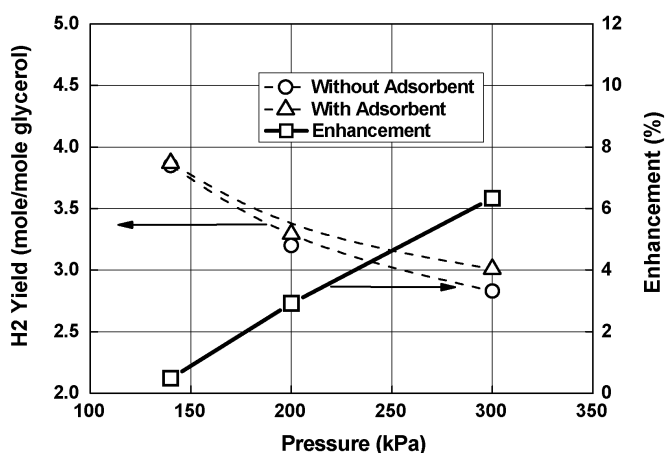
Fig. 21 - Effect of pressure on the hydrogen yield during SEGSR at 450 ºC, WGFR of 9, glycerol/N_2 volume ratio of 0.025, using a Ni-based catalyst and microsized hydrotalcite as CO_2 sorbent. Reprinted from Chemical Engineering Research and Design, 89, Chen H, Ding Y, Cong NT, Dou B, Dupont V, Ghadiri M, et al., Progress in low temperature hydrogen production with simultaneous CO2 abatement, 1774-82, Copyright (2011), with permission from Elsevier.
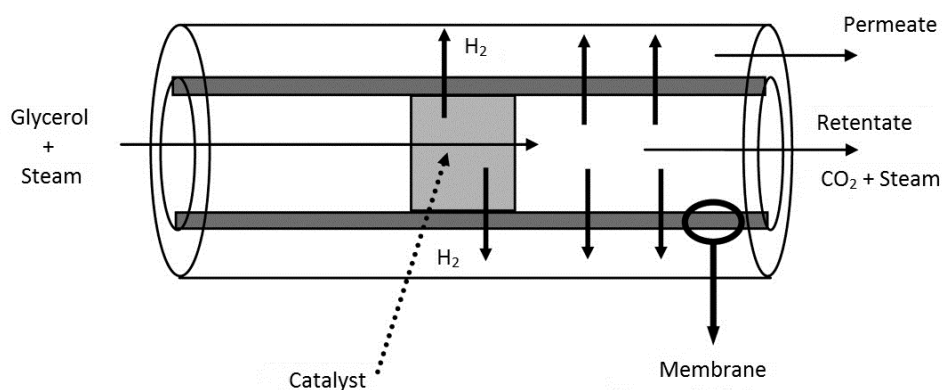
Fig. 22 - Scheme of a MR for the GSR reaction. Adapted from Journal of Catalysis, 252, Haag S, Burgard M, Ernst B., Beneficial effects of the use of a nickel membrane reactor for the dry reforming of methane: Comparison with thermodynamic predictions, 190-204, Copyright (2007), with permission from Elsevier.
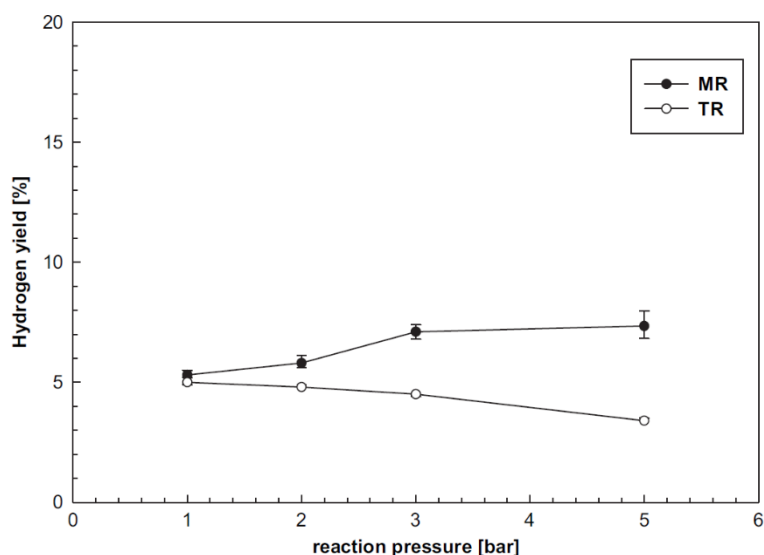
Fig. 23 - Effect of reaction pressure on the hydrogen yield for the traditional reactor (TR) and membrane reactor (MR) at 400 °C, WGFR of 6, WHSV of 1.0 h^{-1}, counter-current configuration of sweep-gas, atmospheric pressure in the permeate side and $Q_{sweep-gas}/Q_{glycerol-in}$=11.9. Reprinted from International Journal of Hydrogen Energy, 36, Iulianelli A, Seelam PK, Liguori S, Longo T, Keiski R, Calabrò V, et al., Hydrogen production for PEM fuel cell by gas phase reforming of glycerol as byproduct of bio-diesel. The use of a Pd–Ag membrane reactor at middle reaction temperature, 3827-34, Copyright (2011), with permission from International Journal of Hydrogen Energy.
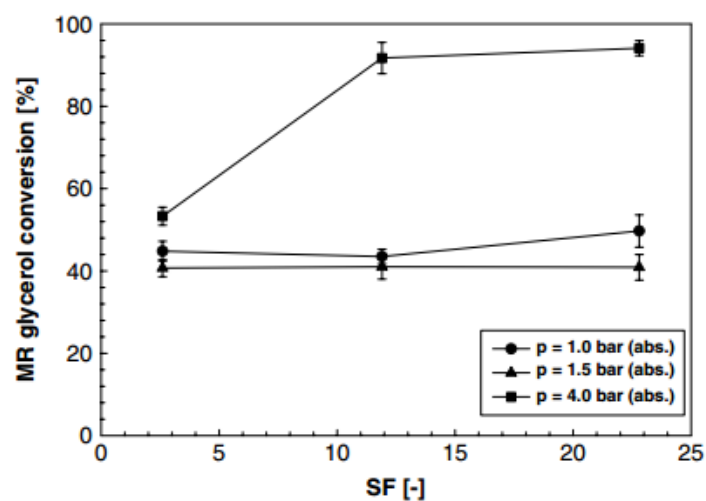
Fig. 24 - Dependency of glycerol conversion the sweep factor (SF) in the Pd-Ag MR at different reaction pressures, 400 ºC, WGFR of 6 and WHSV of 1.01 h^{-1}. Reprinted from Asia-Pacific Journal of Chemical Engineering, 5, Iulianelli A, Longo T, Liguori S, Basile A., Production of hydrogen via glycerol steam reforming in a Pd-Ag membrane reactor over Co-Al2O3 catalyst, 138-45, Copyright © 2009 Curtin University of Technology and John Wiley & Sons, Ltd.

Table 1 - Summary of the catalytic performance and operating conditions of different Ni-based catalysts on GSR.

Catalyst	Operating Conditions	Conversion (%)	Type of Conversion	H_2 Yield (%)[a]/ Selectivity (%)	Reference
11.6 wt.% Ni/CeO$_2$	600 °C, 1 atm, feed flow rate = 0.5 mL·min^{-1} and WGFR = 9	100	Glycerol conversion[b]	n.d.[c]/70	[48]
9.62 wt.% Ni/MgO	600 °C, 1 atm, feed flow rate = 0.5 mL·min^{-1} and WGFR = 9	100	Glycerol conversion[b]	n.d.[c]/40	[48]
12.7 wt.% Ni/TiO$_2$	600 °C, 1 atm, feed flow rate = 0.5 mL·min^{-1} and WGFR = 9	60	Glycerol conversion[b]	n.d.[c]/15	[48]
10 wt.% Ni/ZrO$_2$	650 °C, 1 atm, feed flow rate = 0.06 mL·min^{-1} and 10 wt.% glycerol	72 (20 h)[d]	Glycerol conversion to gaseous products[e]	65/n.d.[c]	[51]
12.6 wt.% Ni/γ-Al$_2$O$_3$	500 °C, 4 atm, WHSV[f] = 7.7 h^{-1} and 10 wt.% glycerol	100 (8 h)[d]	Glycerol conversion[b]	50/n.d.[c]	[53]
10 wt.% Ni/SiC	400 °C, 1 atm, WHSV[f] = 33.3 h^{-1} and WGFR = 9	95.2 (60 h)[d]	Glycerol conversion to gaseous products[e]	n.d.[c]/n.d.[c]	[60]

[a] Based on the thermodynamic limit established in each work;
[b] Calculation based on the total amount of glycerol converted;
[c] n.d.: not determined;
[d] Time of operation after which the data was collected;
[e] Calculation based on the amount of carbon (in glycerol) converted into gaseous products (CO_2, CO and CH_4);
[f] WHSV: weight hourly space velocity.

Table 2 - Summary of the catalytic performance and operating conditions of different promoted Ni-based catalysts on GSR.

Catalyst	Operating Conditions	Conversion (%)	Type of Conversion	H_2 Yield (%)[a] /Selectivity (%)	Reference
8.4% Ni/γ-Al$_2$O$_3$/6 wt.% La$_2$O$_3$	500 ºC, 4 atm, WHSV[b] = 7.7 h^{-1} and 10 wt.% glycerol	100 (8 h)[c]	Glycerol conversion[d]	99.7/n.d.[e]	[22]
11.9 wt% Ni/γ-Al$_2$O$_3$/4.3 wt.% CeO$_2$	500 ºC, 4 atm, WHSV[b] = 7.7 h^{-1} and 10 wt.% glycerol	100 (8 h)[c]	Glycerol conversion[d]	80.3/n.d.[e]	[53]
13.4 wt.% Ni/γ-Al$_2$O$_3$ – 7 wt.% ZrO$_2$	500 ºC, 4 atm, WHSV[b] = 7.7 h^{-1} and 10 wt.% glycerol	100 (7-8 h)[c]	Glycerol conversion[d]	62/n.d.[e]	[65]
10 wt.% Ni/MoLaCa-LTA	600 ºC, feed flow rate = 0.63 mL·min^{-1} and 35 wt.% glycerol	82.03 (100 h)[c]	Glycerol conversion to gaseous products[f]	n.d.[e]/n.d.[e]	[66]

[a] Based on the thermodynamic limit established in each work;
[b] WHSV: weight hourly space velocity;
[c] Time of operation after which the data was collected;
[d] Calculation based on the total amount of glycerol converted;
[e] n.d.: not determined;
[f] Calculation based on the amount of carbon (in glycerol) converted into gaseous products (CO_2, CO and CH_4).

Table 3 - Summary of the catalytic performance and operating conditions of different Pt-based catalysts on GSR.

Catalyst	Operating Conditions	Conversion (%)	Type of Conversion	H$_2$ Yield (%)[a]/ Selectivity (%)	Reference
3 wt.% Pt/Y$_2$O$_3$	600 °C, 1atm, feed flow rate = 0.06 mL·min^{-1}, carrier gas flow rate = 33 mL·min^{-1} and WGFR = 24	100 (2.5-3 h)[b]	Glycerol conversion to gaseous products[c]	90.0/n.d.[d]	[54]
5 % Pt/C	400 °C, 5 atm, volumetric flow rate at reactor inlet = 210 mL·min^{-1} and WGFR = 9	60 (3 h)[b]	Glycerol conversion[e]	37.0/n.d.[d]	[89]
1 wt.% Pt/SiO$_2$	350 °C, 1 atm, Space time = 0.88 min, feed flow rate = 0.5 mL·min^{-1} and 10 wt.% glycerol	85 (2 h)[b]	Glycerol conversion to gaseous products[c]	n.d.[c]/n.d.[d]	[91]
2 wt.% Pt/SiO$_2$	350 °C, 1 atm, Space time = 0.88 min, feed flow rate = 0.5 mL·min^{-1} and 10 wt.% glycerol	100 (2 h)[b]	Glycerol conversion to gaseous products[c]	n.d.[d]/n.d.[d]	[91]
3 wt.% Pt/Al$_2$O$_3$	350 °C, 1 atm, feed flow rate = 0.32 mL·min^{-1} and 30 wt.% glycerol	$\approx$ 21.0	Glycerol conversion to gaseous products[c]	n.d.[d]/n.d.[d]	[92]

[a] Based on the thermodynamic limit established in each work;
[b] Time of operation after which the data was collected;
[c] Calculation based on the amount of carbon (in glycerol) converted into gaseous products (CO$_2$, CO and CH$_4$);
[d] n.d.: not determined;
[e] Calculation based on the total amount of glycerol converted.

Table 4 - Summary of the catalytic performance and operating conditions of different promoted Pt-based catalysts on GSR.

Catalyst	Operating Conditions	Conversion (%)	Type of Conversion	H_2 Yield (%)[a]/ Selectivity (%)	Reference
Pt/4 wt.% CeO_2-1 wt.% ZrO_2-α-Al_2O_3	350 °C, space time = 6 min, feed flow rate = 0.1 mL·min^{-1} and 10 wt.% glycerol	78.0 (1 h)[b]	Glycerol conversion to gaseous products [c]	n.d.[d]/72.5	[97]
3 wt.% Pt/20 wt.% CeO_2/Al_2O_3	350 °C, 1 atm, feed flow rate = 0.32 mL·min^{-1} and 30 wt.% glycerol	88.0	Glycerol conversion to gaseous products [c]	n.d.[d]/n.d.[d]	[92]
3 wt.% Pt/5 wt.% La_2O_3/Al_2O_3	350 °C, 1 atm, feed flow rate = 0.32 mL·min^{-1} and 30 wt.% glycerol	91.0	Glycerol conversion to gaseous products [c]	n.d.[d]/n.d.[d]	[92]

[a] Based on the thermodynamic limit established in each work;
[b] Time of operation after which the data was collected;
[c] Calculation based on the amount of carbon (in glycerol) converted into gaseous products (CO_2, CO and CH_4);
[d] n.d.: not determined.

Table 5 - Summary of the catalytic performance and operating conditions of different non-promoted and promoted Co-based catalysts on GSR.

Catalyst	Operating Conditions	Conversion (%)	Type of Conversion	H_2 Yield (%)[a]/ Selectivity (%)	Reference
15 % Co/CeO$_2$	425 ºC, 1 atm, GHSV[b] = 11 000 mL·g$_{cat.}$$^{-1}$·h^{-1} and G/W/He[c] = 2/18/80 vol.%	100	Not specified	n.d.[d]/88.0	[106]
15 wt.% Co/Al$_2$O$_3$	500 ºC, 1 atm, GHSV[b] = 50 000 mL·g$_{cat.}$$^{-1}$·h^{-1} and p$_{glycerol}$ = 7.40 kPa and p$_{steam}$ = 57.02 kPa	≈ 13.0	Glycerol conversion to gaseous products[e]	77.0[f]/63.0	[107]
5 wt.% Co-10 wt.% Ni/Al$_2$O$_3$	525 ºC, 1 atm, GHSV[b] = 50 000 mL·g$_{cat.}$$^{-1}$·h^{-1} and 30 wt.%	-	-	79.1/65.3	[108]

[a] Based on the thermodynamic limit established in each work;
[b] GHSV: gas hourly space velocity;
[c] G/W/He: glycerol/water/helium volumetric composition;
[d] n.d.: not determined;
[e] Calculation based on the amount of carbon (in glycerol) converted into gaseous products (CO_2, CO and CH_4);
[f] Assuming a thermodynamic limit of 7.

Table 6 - Summary of the catalytic performance and operating conditions of different non-promoted and promoted Ru-based catalysts on GSR.

Catalyst	Operating Conditions	Conversion (%)	Type of Conversion	H_2 Yield (%)[a]/ Selectivity(%)	Reference
5 % Ru/Al$_2$O$_3$	400 ℃, 1 atm, feed flow rate = 0.20 mL·min^{-1} and WGFR = 9	68.1 (2 h)[b]	Glycerol conversion[c]	37.0/n.d.[d]	[114]
3 wt.% Ru/Y$_2$O$_3$	600 ℃, 1 atm, GHSV[e] = 80 000 mL·g$_{cat.}$$^{-1}$·h^{-1} and WGFR = 9	≈ 100 (24 h)[b]	Glycerol conversion to gaseous products[f]	85/90.0[g]	[117]
0.59 wt.% Ru- 0.23 wt.% Sn/Mg(Al)O	650 ℃, 1 atm, feed flow rate = 0.06 mL·min^{-1} and 10 wt.% glycerol	87.5 (20 h)[b]	Glycerol conversion to gaseous products[f]	60/n.d.[d]	[120]
0.06 wt.% Ru/Mg(Al)O	550 ℃, 1 atm, WHSV[h] = 327.3 h^{-1}[i] and 10 wt.% glycerol	97 (20 h)[b]	Glycerol conversion to gaseous products[f]	91.0/97.0[j]	[121]

[a] Based on the thermodynamic limit established in each work;
[b] Time of operation after which the data was collected;
[c] Calculation based on the total amount of glycerol converted;
[d] n.d.: not determined;
[e] GHSV: gas hourly space velocity;
[f] Calculation based on the amount of carbon (in glycerol) converted into gaseous products (CO_2, CO and CH_4);
[g] taken from [122];
[h] WHSV: weight hourly space velocity;
[i] Calculated value;
[j] CO_2 selectivity.

Table 7 - Summary of the catalytic performance and operating conditions of different noble metal-based catalysts on GSR.

Catalyst	Operating Conditions	Conversion (%)	Type of Conversion	H$_2$ Yield (%)[a]/ Selectivity (%)	Reference
Ir/CeO$_2$	400 °C, 1 atm, GHSV[b] = 11 000 mL·g$_{cat.}^{-1}$·h^{-1} and G/W/He[c] = 2/18/80 vol.%	100	Not specified	n.d.[d]/85.6	[106]
5 wt.% Rh/Al$_2$O$_3$	650 °C, 1 atm, GHSV[b] = 5000 h^{-1} and WGFR = 9	50.0 (100 h)[e]	Glycerol conversion to gaseous products[f]	35.7[g]/n.d.[d]	[128]
1 wt.% Pd/Al$_2$O$_3$	600 °C, 1 atm, feed flow rate = 0.05 mL·min^{-1} and WGFR = 6	80.0 (2 h)[e]	Glycerol conversion to gaseous products[f]	55.0/70.0	[133]
10 wt.% Ce/Al$_2$O$_3$	600 °C, 1 atm, feed flow rate = 0.05 mL·min^{-1} and WGFR = 6	55.0 (2 h)[e]	Glycerol conversion to gaseous products[f]	42.0/80.0	[133]

[a] Based on the thermodynamic limit established in each work;
[b] GHSV: gas hourly space velocity;
[c] G/W/He: glycerol/water/helium volumetric composition;
[d] n.d.: not determined;
[e] Time of operation after which the data was collected;
[f] Calculation based on the amount of carbon (in glycerol) converted into gaseous products (CO_2, CO and CH_4);
[g] Assuming a thermodynamic limit of 7.

Table 8 - Activation energies and reaction orders for the GSR reaction over different catalyst.

Catalyst	Operating conditions[a]	Preparation method	E_a (kJ·mol^{-1})	Reaction order for glycerol[b]	Reaction order for steam[b]	Reference
15 wt.% Ni- 10 wt.% ZrO_2/CeO_2	1 atm, 600 – 700 °C	Wet impregnation of CeO_2 with $Ni(NO_3)_2 \cdot 6H_2O$ and $ZrO(NO_3)_2 \cdot xH_2O$ aqueous solutions	43.4	0.3	0	[18]
24.1 wt.% Ni- 26.1 wt.% Mg- 49.8 wt.% Al	1 atm, 400 - 600 °C	Co-precipitation method with rising pH technique using $Ni(NO_3)_2 \cdot 6H_2O$, $Al(NO_3)_3 \cdot 9H_2O$ and $Mg(NO_3)_2 \cdot 6H_2O$ aqueous solutions	37.8	1.0 (WGFR = 9)	0	[24]
15 wt.% Ni/CeO_2	1 atm, 400-700 °C[c]	Deposition-precipitation using Ni $(NO_3)_2 \cdot 6H_2O$ aqueous solution	36.5	n.d.[d]	n.d.[d]	[50]
15 wt.% Ni/Al_2O_3	1 atm, 450– 550 °C	Wet impregnation of γ-Al_2O_3 with Ni $(NO_3)_2 \cdot 6H_2O$ aqueous solution	59.8	0.48 (30 – 60 wt.%)	0.34 (40 – 70 wt.%)	[134]
Ni/CeO_2[c]	1 atm, 600 – 650 °C	Wet impregnation of CeO_2 with Ni $(NO_3)_2 \cdot 6H_2O$ aqueous solution	103.4	0.23	0	[135]
15 wt.% Co/Al_2O_3	1 atm, 450 – 550 °C	Wet impregnation of Al_2O_3 with Co $(NO_3)_2 \cdot 6H_2O$ aqueous solution	67.2	0.08 (30 – 60 wt.%)	0.39 (40 – 70 wt.%)	[107]
5 wt.% Co-10 wt.% Ni/Al_2O_3	1atm, 500 – 550 °C	Co-impregnation of Al_2O_3 with $Co(NO_3)_2 \cdot 6H_2O$ and $Ni(NO_3)_2 \cdot 6H_2O$ aqueous solutions	63.3	0.25 (4.5-16.5 kPa)	0.36 (25-88 kPa)	[108]
Pt/C	5 atm , 350 – 400 °C	Supplied by Arora-Matthey Ltd., Kolkata	n.d.[d]	1.0 (10-34 kPa)	0	[89]
5% Ru/Al_2O_3	1 atm, 350 – 500 °C	Supplied by Johnson-Matthey Ltd., Delhi.	21.2	1.0 (x_G = 0.068-0.091)	0	[114]

[a] – Temperature and total pressure at which the experiments were carried out;
[b] – The values between brackets are the ranges of each species in the feed or their partial pressure;
[c] – Metal loading not specified;
[d] n.d.: not determined.

Table 9 - Sorption capacities and sorption/regeneration temperatures of several CO_2 sorbents reported in the literature for SERs applications.

Sorbent	Sorption capacity (mol/kg)	Sorption temperature (°C)	Regeneration temperature (°C)	p_{CO_2} (bar)	p_{H_2O} (bar)	Reference
K-doped hydrotalcite (20 wt.% K_2CO_3 and Mg/Al ratio = 2)	9.40[a]	300	600	0.34	4.5	[141]
K-Na-doped hydrotalcite	1.11[a]	300	300	0.40	0.42	[142]
Hydrotalcite	1.18	400	n.s.	0.15	0	[164]
Ga-K-doped hydrotalcite (10 wt.% Ga and 20 wt.% K)	1.82	300	300	1.08	0	[165]
CaO-Y_2O_3 (20 wt.% Y_2O_3)	12.95	850	850	n.s.[b]	0	[147]
CaO from calcium acetate	17.30	600	700	0.30	0	[164, 166]
Dolomite	8.40	750	n.s.	0.15	n.s.[b]	[164]
Li_2ZrO_3	5.00[a]	500	n.s.	n.s.[bc]	n.s.[bc]	[153]
K-doped Li_4SiO_4 (30 wt.% K_2CO_3)	5.23	580	700	0.04	0	[156]
Li_4SiO_4 (treated with glacial acetic acid)	0.77	550	625	0.1	0	[157]

[a] Wet conditions;
[b] n.s.: not specified;
[c] – Total pressure = 4.47 bar.

Table 10 – Characteristics of different Pd-based membranes reported in the literature.

Membrane	T (ºC)[a]	ΔP (kPa)[b]	δ (µm)	Permeance to H_2 ($mol \cdot m^{-2} \cdot s^{-1} \cdot Pa^{-0.5}$)	Ideal selectivity H_2/N_2	$E_{a,Pd}$ ($kJ \cdot mol^{-1}$)	Reference
Pd-25 wt.% Ag	300	10-150	50	1.15×10^{-4c}	∞	10.72	[180]
Pd-23-25 wt.% Ag	350	700	84	2.26×10^{-4c}	∞	2.92	[181]
$Pd_{46.6}$-$Cu_{53.4}$	400	345	40	4.50×10^{-4c}	-	5.80	[182]
$Pd_{45.8}$-$Cu_{51.9}$-$Ag_{2.3}$	400	345	40	$3.50 \times 10-4^{c}$	-	10.20	[182]
Pd-5 wt.% Pt/YSZ	400	57.9-609.5	6.6	1.18×10^{-3c}	994	-	[183]
Pd/Ag/PSS	400	100	4.0	1.71×10^{-3c}	1000	11.90	[184]
Pd/Pencil/PSS	450	100	7.0	1.40×10^{-3c}	120	13.80	[185]
$Pd/TiO_2/Ti$-Al	500	588-704[c]	14.0	1.07×10^{-3}	∞	13.65	[186]
$Pd_{78}Ag_9Au_{13}$	450	-	14.0	1.16×10^{-3c}	-	-	[187]
$Ti_{50.864}Ni_{46.961}Pd_{4.175}$	450	100	45.0	3.84×10^{-6c}	-	42.23	[188]
$Pd_{95}Au_5$	400	-	2.5	4.40×10^{-3c}	$\geq 10\ 000$	-	[189]
$Pd_{95}Y_5$	400	-	2.0	5.50×10^{-3c}	$\geq 10\ 000$	-	[189]
$Pd_{73}Cu_{26}Y_1$	400	-	2.0	2.50×10^{-3c}	$\geq 10\ 000$	-	[189]

YSZ: Yttria-stabilized zirconia;
PSS: Porous stainless steel;
[a] Temperature at which the permeance was obtained;
[b] Trans-membrane pressure difference at which the permeance was obtained;
[c] Calculated values.